



Decellularized Disc Hydrogels for hBMSCs tissue-specific differentiation and tissue regeneration

Yizhong Peng^{a,1}, Xiangcheng Qing^{a,1}, Hui Lin^{a,1}, Donghua Huang^b, Jinye Li^a, Shuo Tian^a, Sheng Liu^a, Xiao Lv^a, Kaige Ma^a, Rui Li^c, Zilong Rao^c, Ying Bai^d, Songfeng Chen^e, Ming Lei^{a,***}, Daping Quan^{c,d,**}, Zengwu Shao^{a,*}

^a Department of Orthopaedics, Union Hospital, Tongji Medical College, Huazhong University of Science and Technology, Wuhan, 430022, China

^b Musculoskeletal Tumor Center, Department of Orthopaedics, The Second Affiliated Hospital of Zhejiang University School of Medicine, Hangzhou, China

^c School of Chemistry, Sun Yat-sen University, Guangzhou, 510127, China

^d School of Materials Science and Engineering, Sun Yat-sen University, Guangzhou, 510127, China

^e Department of Orthopaedic Surgery, The First Affiliated Hospital of Zhengzhou University, Zhengzhou City, 450052, China

ARTICLE INFO

Keywords:

Tissue specificity
Decellularized tissue matrix
Intervertebral disc
Differentiation
YAP1

ABSTRACT

Tissue specificity, a key factor in the decellularized tissue matrix (DTM), has shown bioactive functionalities in tuning cell fate—e.g., the differentiation of mesenchymal stem cells. Notably, cell fate is also determined by the living microenvironment, including material composition and spatial characteristics. Herein, two neighboring tissues within intervertebral discs, the nucleus pulposus (NP) and annulus fibrosus (AF), were carefully processed into DTM hydrogels (abbreviated DNP-G and DAF-G, respectively) to determine the tissue-specific effects on stem cell fate, such as specific components and different culturing methods, as well as in vivo regeneration. Distinct differences in their protein compositions were identified by proteomic analysis. Interestingly, the fate of human bone marrow mesenchymal stem cells (hBMSCs) also responds to both culturing methods and composition. Generally, hBMSCs cultured with DNP-G (3D) differentiated into NP-like cells, while hBMSCs cultured with DAF-G (2D) underwent AF-like differentiation, indicating a close correlation with the native microenvironments of NP and AF cells, respectively. Furthermore, we found that the integrin-mediated RhoA/LATS/YAP1 signaling pathway was activated in DAF-G (2D)-induced AF-specific differentiation. Additionally, the activation of YAP1 determined the tendency of NP- or AF-specific differentiation and played opposite regulatory effects. Finally, DNP-G and DAF-G specifically promoted tissue regeneration in NP degeneration and AF defect rat models, respectively. In conclusion, DNP-G and DAF-G can specifically determine the fate of stem cells through the integrin-mediated RhoA/LATS/YAP1 signaling pathway, and this tissue specificity is both compositional and spatial, supporting the utilization of tissue-specific DTM in advanced treatments of intervertebral disc degeneration.

1. Introduction

Intervertebral disc degeneration (IDD) is one of the most common

diseases that disturbs the musculoskeletal system [1]. However, the commonly used clinical treatments, such as surgical operations, local blocking and medical conservative therapies, have not reached certain

Abbreviations: IDD, intervertebral disc degeneration; DTM, decellularized tissue matrix; NP, nucleus pulposus; AF, annulus fibrosus; MSC, mesenchymal stem cell; 2D, two-dimensional; 3D, three-dimensional; YAP1, yes-associated protein 1; FNP, fresh nucleus pulposus; FAF, fresh annulus fibrosus; DNP, decellularized nucleus pulposus; DAF, decellularized annulus fibrosus; DNP-G, decellularized nucleus pulposus hydrogel; DAF-G, decellularized annulus fibrosus hydrogel; ECM, extracellular matrix; Col I-S, collagen type I solution; DNP-S, decellularized nucleus pulposus solution; DAF-S, decellularized annulus fibrosus solution.

Peer review under responsibility of KeAi Communications Co., Ltd.

* Corresponding author.

** Corresponding author. School of Chemistry, Sun Yat-sen University, Guangzhou, 510127, China.

*** Corresponding author.

E-mail addresses: seveage@126.com (M. Lei), cesqdp@mail.sysu.edu.cn (D. Quan), szwpro@163.com, 1985xh0536@hust.edu.cn (Z. Shao).

¹ Yizhong Peng, Xiangcheng Qing and Hui Lin contributed equally to this work and shall share first authorship.

<https://doi.org/10.1016/j.bioactmat.2021.03.014>

Received 24 December 2020; Received in revised form 2 March 2021; Accepted 2 March 2021

2452-199X/© 2021 The Authors. Publishing services by Elsevier B.V. on behalf of KeAi Communications Co. Ltd. This is an open access article under the CC

BY-NC-ND license (<http://creativecommons.org/licenses/by-nc-nd/4.0/>).

satisfaction [2]. Thus, seeking new therapeutic strategies for IDD is an urgent mission for clinical researchers.

Biomaterial-based therapy, by focusing on biomechanical restoration, has drawn increased attention in recent decades. The intervertebral disc comprises three significantly different tissues, the nucleus pulposus (NP), annulus fibrosus (AF) and cartilage endplate [3]. Among them, NP and AF are the main tissues for withstanding the mechanical stress and mobility of the spine [4]. Therefore, biomaterials designed for intervertebral disc regeneration are mainly considered to repair NP or AF [5]. NP repair restores the motion characteristics and physical properties of the target segments by NP tissue rehydration or NP replacement [6]. Biomaterials for NP replacement have focused mainly on injectable synthetic or biologically based hydrogels [7–9]. These hydrogels are mainly derived from non-degradable polyacrylates and polyacrylamides [10,11] and degradable hyaluronic acid, collagen in the extracellular matrix and chitosan [8,12]. However, these implanted materials often failed to regulate the post-injury microenvironment, and tissue degeneration, water loss and inflammatory reaction often appeared in situ [13,14]. Regarding AF, structural repair is a hot spot. Many strategies have been proposed to repair the herniation site, including mesh attachment, void filling, and collagen reconstruction [15–17]. However, biomaterials designed for the regeneration and integrity of AF defects have not yet observed satisfying clinical outcomes [5].

Recently, an increasing number of studies have been conducted to assess the effects of cell therapy for IDD [18]. Several favorable results have been observed for stem cell therapy of IDD. Although transplanted mesenchymal stem cells (MSC) can differentiate into intervertebral disc (IVD) cells and significantly promote extracellular matrix (ECM) synthesis in IVD tissues [19] and improve the clinical outcome of IDD patients [20], unexpected findings such as a low survival rate and uncontrolled multidirectional differentiation of MSCs were observed in some studies without suitable carrier materials [21,22].

Many studies have shown that the decellularized tissue matrix (DTM) can remove immunogenicity and retain most of the functional compositions (cytokines, matrix-bound nanovesicles, or peptides) and micro/nanostructure of the native tissue [23]. Hydrogels derived from different DTM have attracted increased attention such as implanting them directly into the body to facilitate regeneration or as a carrier of cells, drugs and other proteins through a minimally invasive injection [23]. More interestingly, DTM hydrogels can not only function as physical carriers but also have tissue specificity that regulates cell fate. For example, decellularized extracellular matrix hydrogels derived from the liver, heart, skin and cornea induced tissue-specific gene patterns in human bone marrow mesenchymal stem cells (hBMSCs) [24]. Urea-extracted DTM hydrogels from tendons and cartilage induced the multi-directional differentiation of mesenchymal stem cells (MSCs) with different gene expression patterns, in which the TGF- β signaling pathway might be engaged in this tissue-specific effect [25]. A hydrogel derived from the spinal cord (DSCM-gel) facilitated neural stem/progenitor cells (NSPCs) differentiation into neurons using an in vitro 3D cultural model and provided a suitable microenvironment for endogenous stem/progenitor cell recruitment in vivo [26]. Inspired by these results, we speculated how decellularized NP and AF hydrogels (denoted DNP-G and DAF-G, respectively) affect the fate of MSCs without adding external factors when these two types of hydrogel materials are used as MSC carriers. This information is critical to apply this type of material in a suitable form (hydrogel or electrospun fibers) in IDD repair in vivo (with/without stem cells). Additionally, NP is a centralized fibrogelatinous core comprising aggrecan and collagen type II, while AF comprises a multilayer structure of aligned collagen type I [27,28]. How do the differences between NP and AF tissues in composition and spatial microstructure play a role in the differentiation of MSCs into NP-like cells or AF-like cells?

In addition to compositional variation, the spatial characteristics of the cell living microenvironment also alter the cell fate of stem cells. Several studies have shown that the three-dimensional (3D)

environment provides additional stimuli for osteogenic differentiation [29–31]. Recent studies have found that NSPCs differentiated into neurons for 3D culture, while NSPC differentiation into astrocyte-like cells became more significant using two-dimensional (2D) culture [26,32]. Additionally, 2D and 3D cultures showed significant differences in myofibroblast differentiation properties. Specifically, in contrast to findings on 2D hydrogels, myofibroblast differentiation in 3D was inversely correlated with hydrogel stiffness but positively correlated with matrix fibers [33]. Therefore, the spatial characteristics of the cellular microenvironment generated by NP and AF hydrogels, particularly the culture microenvironments (2D and 3D), might also significantly influence stem cell differentiation, considering the differences in the microenvironment of NP and AF cells, which have received little attention so far.

In this study, two hydrogels (DNP-G and DAF-G) were fabricated from decellularized NP and AF tissues and the components of these hydrogels were confirmed using proteomic analysis. To investigate the role of environmental characteristics on hBMSCs behaviors, including proliferation and directed differentiation, isolated hBMSCs were co-cultured with DNP-G and DAF-G in 2D/3D models, respectively. Next, integrin/Rho/YAP1 signaling was evaluated, and YAP1 regulation was performed to identify its role in directing hBMSCs differentiation correlated to the compositional and spatial specificity of the environment. Finally, we assessed the different regenerative efficacies of DNP-G and DAF-G on the IDD model (Fig. 1).

2. Results

2.1. Decellularization, fabrication and characterization of DNP-G and DAF-G

After the decellularization of fresh NP and AF (denoted as FNP and FAF, respectively), hematoxylin and eosin (H&E) staining showed almost complete removal of the cell nuclei and a loose extracellular structure in both the DNP and DAF (Fig. 2a). Similarly, immunostaining by DAPI showed that most of the cellular contents were removed (Fig. 2b). Compared with the DNA content in FNP and FAF (241.61 ± 37.16 ng/mg and 306.99 ± 16.25 ng/mg, respectively), the residual DNA contents in DNP and DAF were 23.09 ± 8.51 ng/mg and 22.91 ± 6.72 ng/mg, respectively, which were both lower than the internationally recognized criterion (50 ng/mg) [34], suggesting the high efficiency of our protocol for decellularization processing (Fig. 2c). Because glycosaminoglycan (GAG) and collagen comprises the major components of the ECM, GAG and collagen quantitative analysis was applied to assess the retention of ECM components after decellularization. The GAG quantitative values for FNP, DNP, FAF and DAF were 13.65 ± 0.25 μ g/mg, 10.32 ± 1.36 μ g/mg, 4.88 ± 0.77 μ g/mg, and 3.99 ± 0.11 μ g/mg, respectively (Fig. 2d). The collagen contents for FNP, DNP, FAF and DAF were 80.28 ± 7.27 μ g/mg, 54.07 ± 4.02 μ g/mg, 86.4 ± 4.88 μ g/mg, and 70.34 ± 8.05 μ g/mg, suggesting that the majority of ECM components was preserved after decellularization (Fig. 2e).

SEM analysis was performed to identify the DTM microstructure. Compared with the nanofiber diameters of FNP (91.82 ± 9.12 nm) and FAF (98.12 ± 12.07 nm), DNP-G and DAF-G also showed adequate assembled fibrous structures after decellularization, digestion and gelation. The size of nanofibers increased slightly to 89.1 ± 12.64 nm and 104.38 ± 23.04 nm (Fig. 2f). Additionally, the nanofibers in the DAF were more aligned, and the diameter of the nanofibers was slightly larger than that of the DNP. After gelation, DNP-G and DAF-G formed adhesive, semi-transparent, and stable hydrogels (Fig. 2g), and the storage modulus (G') of DAF-G increased sharply with time until a plateau was reached. This sol-gel transition lasted 1.5 ± 0.9 min, and the maximum G' was reached at 181.18 ± 0.83 Pa. However, the G' of DNP-G was 150.10 ± 3.65 Pa with a much longer gelation period (4 ± 0.4 min).

The composition and functional proteins of both DNP-G and DAF-G

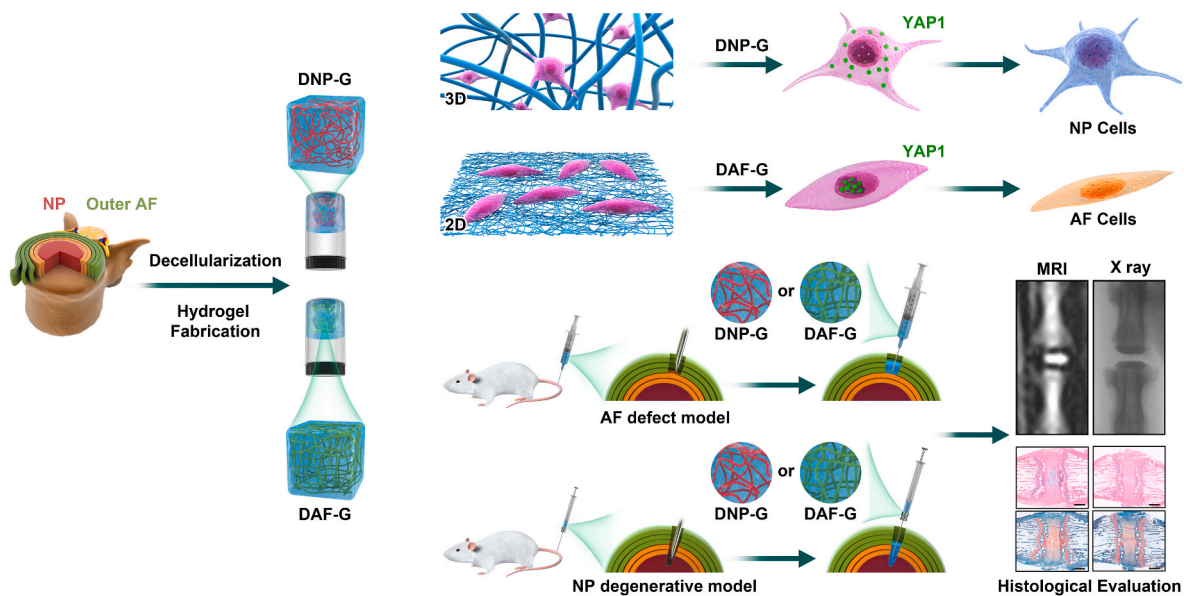


Fig. 1. Schematic diagram of decellularized matrix fabrication and in vitro and in vivo applications.

were analyzed and compared using proteomic analysis. Although the percentage of extracellular matrix (ECM) proteins in DAF-G ($25.79 \pm 4.72\%$) was larger than that in DNP-G ($17 \pm 9.52\%$) (Fig. 2h), the total number of proteins detected in DNP-G (392) was much higher than that in DAF-G (142), and the number of exclusive proteins was 269 for DNP-G and only 19 for DAF-G (Fig. 2i). The most abundant collagen types in DNP-G were COL2A1, COL11A2 and COL9A3. COL1A2 and COL12A1 were commonly found in DAF-G, indicating a significant compositional difference between DNP-G and DAF-G. Secreted factors also significantly varied between DNP-G and DAF-G (Fig. 2i). Functional analysis based on the gene ontology (GO) database indicated that proteins in DNP-G were more abundant than those in DAF-G and were related to “glycosaminoglycan binding”, “protein dimerization activity”, “catalytic activity”, “structural molecule activity” and “carbohydrate derivative binding” and others. However, DAF-G was highly associated with “protein heterodimerization activity” (Fig. 2j). A higher percentage of ECM proteins (Fig. 2g) in DAF-G may contribute to enhanced protein interactions (“protein heterodimerization activity”), such as in DAF-G, fast gelation property, higher elastic modulus, and more condensed nanostructure of DAF-G.

Live/dead staining and CCK8 assays showed that hBMSCs seeded on culture plates (control), Col I, DNP-G and DAF-G all exhibited excellent viability with good spreading and cell distribution (Supplementary Fig. 1a–b), suggesting good cytocompatibility of all biomaterials for cell culture. To further evaluate the immunogenicity and biocompatibility in vivo, a subcutaneous xenograft model was applied. Histological staining showed that the inflammatory cells in the DNP-G and DAF-G groups were less obvious (Supplementary Fig. 1c). Thus, the decellularized matrix derived from NP and AF tissues revealed good biocompatibility.

2.2. Directing hBMSCs differentiation by DNP-G and DAF-G

To distinguish NP cells from AF cells differentiated from hBMSCs, specific markers were first confirmed. NP cells expressed higher levels of COL2A1, CD24, KRT19, ACAN, and NCAM1 than AF cells; thus, they could be considered NP-specific markers (Supplementary Fig. 9). Additionally, COL1A1, COL5A1, IBSP, FBLN1 and TNMD were significantly higher in AF cells than in NP cells (Supplementary Fig. 2, Supplementary Table 1). To evaluate the effects of different components in DNP and DAF on hBMSCs differentiation, the digested fluid (0.015% w/v) of DNP and DAF were added to the cultured media of hBMSCs, using Col I

solution (same concentration) as the control. Safranin O-fast Green (S&O) staining and immunohistochemical analysis showed an increased proteoglycan content in the DNP group but not in the Col I and DAF groups (Fig. 3a). The DNP group showed more positive staining of the NP-specific markers, including CD24 and COL2A1, than that of the other groups. Positive staining of the AF-specific marker COL1A1 was obvious in DAF and Col I groups, and TNMD staining was more obvious in DAF group (Fig. 3a). Therefore, the components in the two digestive solutions derived from DNP and DAF may promote the differentiation of hBMSCs into NP-like cells and AF-like cells, respectively.

hBMSCs were encapsulated in both hydrogels (3D) or seeded on hydrogel pre-coated culture plates (2D) to further confirm the influence of DNP-G and DAF-G on hBMSCs tissue-specific differentiation. NP-specific markers, including COL2A1, CD24, KRT19, ACAN, and NCAM1, were upregulated when hBMSCs were cultured in DNP-G (3D or 2D culture) for 21 days, although CD24 and NCAM1 were not significantly different between DNP-G and DAF-G for 2D culturing (Fig. 3b). Additionally, the emission intensity of the NP-specific marker GPC3 was increased in DNP-G, particularly for 3D culturing (Fig. 3c–d). These results indicated that DNP-G promoted hBMSCs differentiation into NP-like cells potentially with preference for 3D. Because the culture microenvironments (2D or 3D) may also play a critical role in the specific differentiation of cultured hBMSCs, we compared the effects of the culturing microenvironment (2D or 3D) on hBMSCs differentiation by RT-qPCR, which revealed that the DNP-G 3D microenvironment significantly promoted NP-specific markers expression (Fig. 3e).

However, when cultured in DAF-G, hBMSCs showed higher expression of AF-specific markers, except for COL1A1 and FBLN1, in the 3D microenvironment (Fig. 4a). The intensity of the AF-specific marker TNMD was also higher than that of the other groups, mainly for 2D culturing (Fig. 4b–c), implying that hBMSCs differentiate into AF-like cells. Next, compared with the 3D microenvironment, hBMSCs expressed more AF-specific markers when cultured on the surface of DAF-G (Fig. 4d). Therefore, the tissue-specific differentiation of hBMSCs can not only be directed by DNP-G and DAF-G compositions but also by the spatial specificity of different culture microenvironments.

2.3. The integrin-mediated RhoA/LATS/YAP1 signaling pathway is triggered by DAF-G in 2D manner

Integrin-transduced Hippo/YAP1 signaling senses cell adhesion and

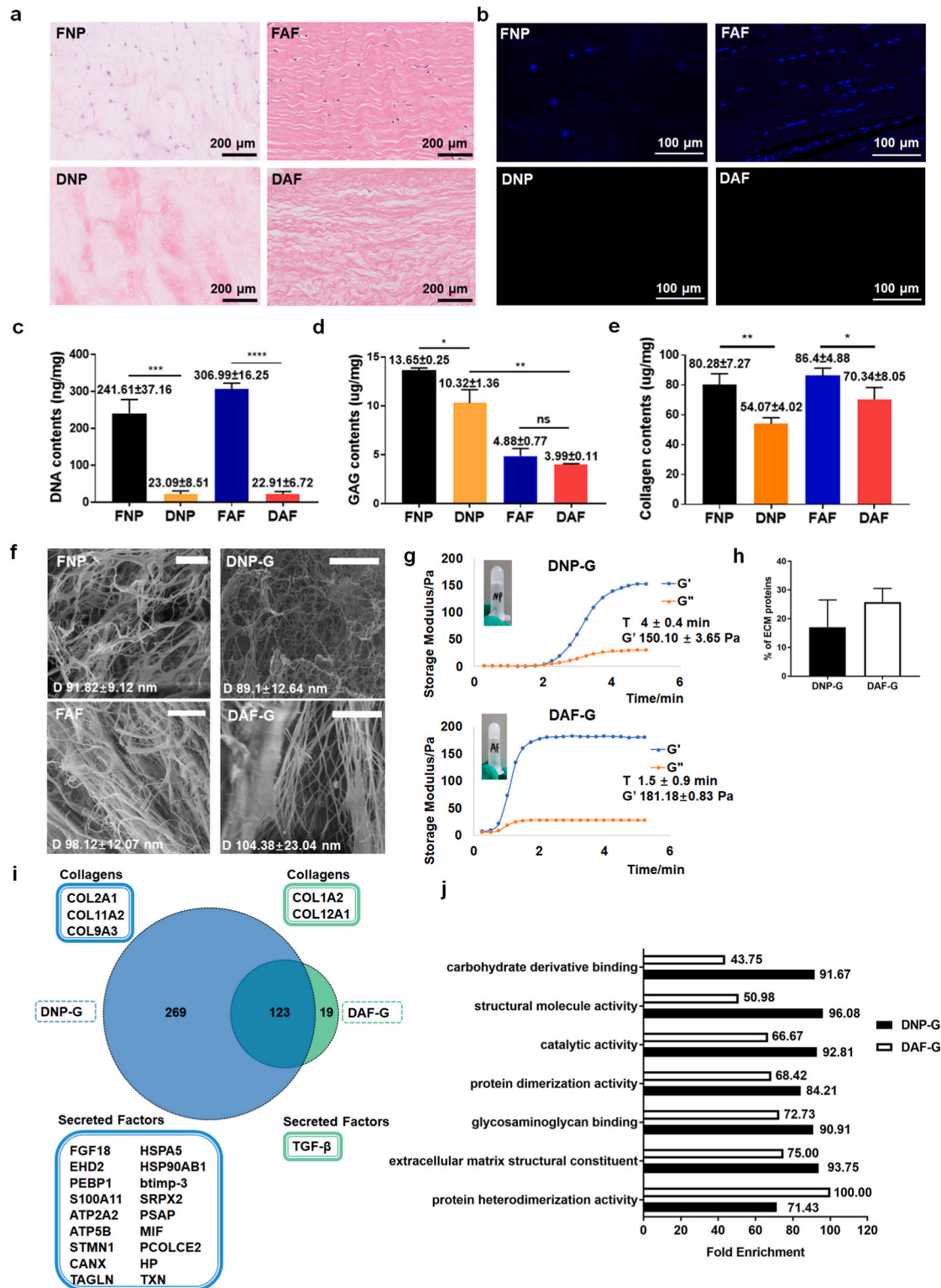


Fig. 2. Differences in characteristics and proteomic analysis of DNP-G and DAF-G. **a** H&E staining of FNP, FAF, DNP and DAF showed that the cellular component was largely removed and the extracellular matrix was preserved. **b** DAPI staining also suggested the removal of cellular components to a large extent. **c** the efficacy of cellular removal detected by DNA contents. The remaining extracellular components detected by **d** GAG measurement and **e** collagen content. **f** SEM analysis showed the ultrastructure of the materials. (Scale bar = 10 μm) **g** General appearance and rheological behavior of DNP-G and DAF-G. **h** The percentages of total proteins that ECM proteins accounted for in DNP-G and DAF-G. **i** Protein variety comparison between DNP-G and DAF-G. **j** Molecular function comparison between DNP-G and DAF-G. (Data are presented as the mean ± SD, n = 3, *p < 0.05, **p < 0.01, ****p < 0.0001 between two groups; ns, no significance.) FNP, fresh nucleus pulposus; FAF, fresh annulus fibrosus; DNP, decellularized nucleus pulposus; DAF, decellularized annulus fibrosus; DNP-G, decellularized nucleus pulposus hydrogel; DAF-G, decellularized annulus fibrosus hydrogel; ECM, extracellular matrix.

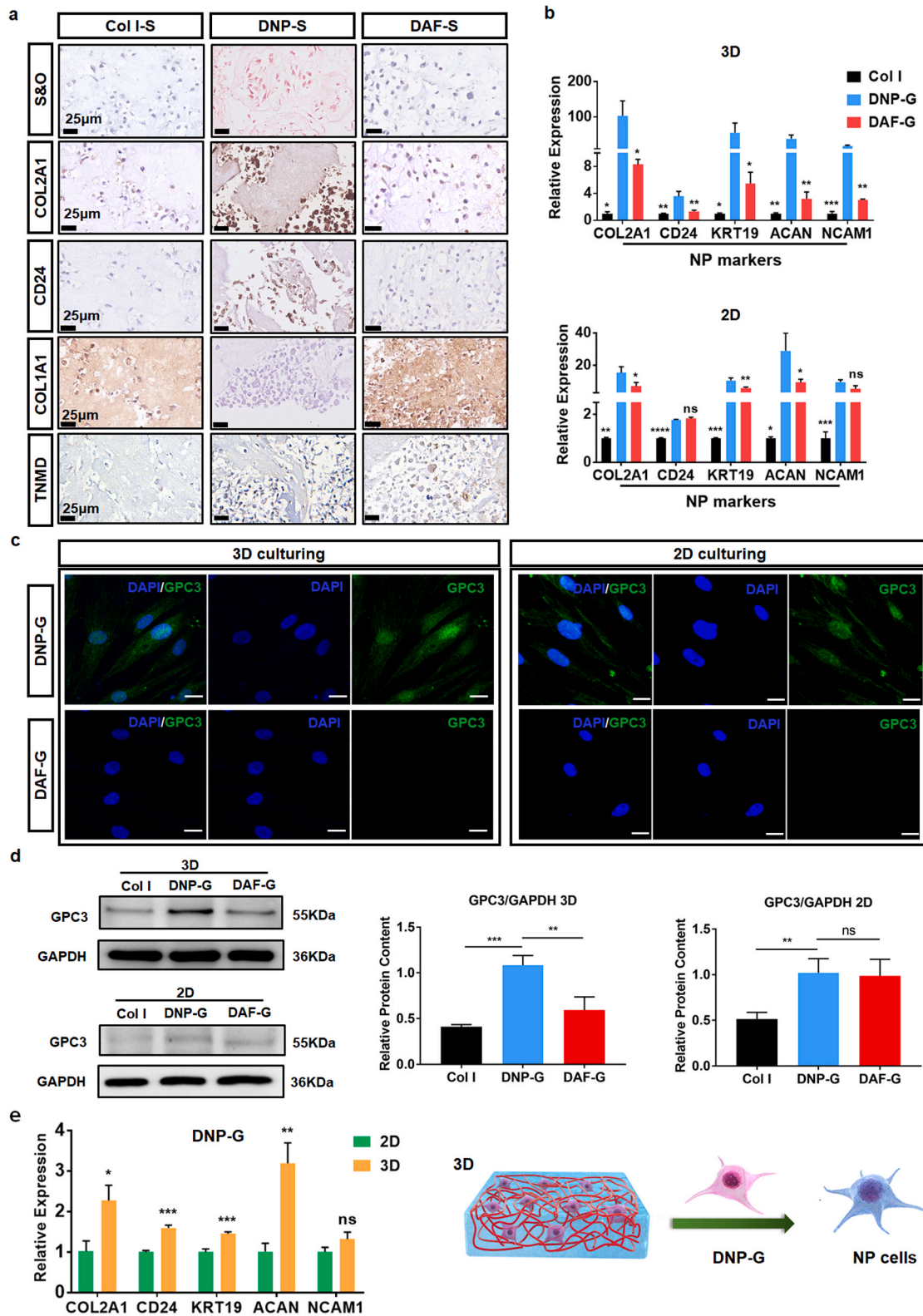


Fig. 3. Composition-specific and space-specific differentiation of hBMSCs cultured in DTM. **a** S&O staining and anti-CD24, anti-COL2A1, anti-COL1A1 and anti-TNMD immunostaining of hBMSCs pellets cultured in 0.015% ($w v^{-1}$) Col I-S, DNP-S and DAF-S. (Scale bar = 500 μm and 25 μm for low and high magnification) **b** RT-qPCR of NP-specific markers in hBMSCs cultured in Col I, DNP-G and DAF-G under 3D or 2D culture. (Data are presented as the mean \pm SD, $n = 3$, * $p < 0.05$, ** $p < 0.01$, *** $p < 0.001$, **** $p < 0.0001$ between DNP-G and other groups; ns, no significance.) **c** Immunofluorescence of GPC3 in hBMSCs cultured in DNP-G and DAF-G under 3D or 2D microenvironment. (Scale bar = 20 μm) **d** Western blots and grayscale analysis of GPC3. **e** Differential expression of NP-specific markers expression in hBMSCs between 2D and 3D microenvironments. Col I-S, collagen type I solution; DNP-S, decellularized nucleus pulposus solution; DAF-S, decellularized annulus fibrosus solution. (Data are presented as the mean \pm SD, $n = 3$, * $p < 0.05$, ** $p < 0.01$, *** $p < 0.001$, **** $p < 0.0001$ between two groups; ns, no significance.)

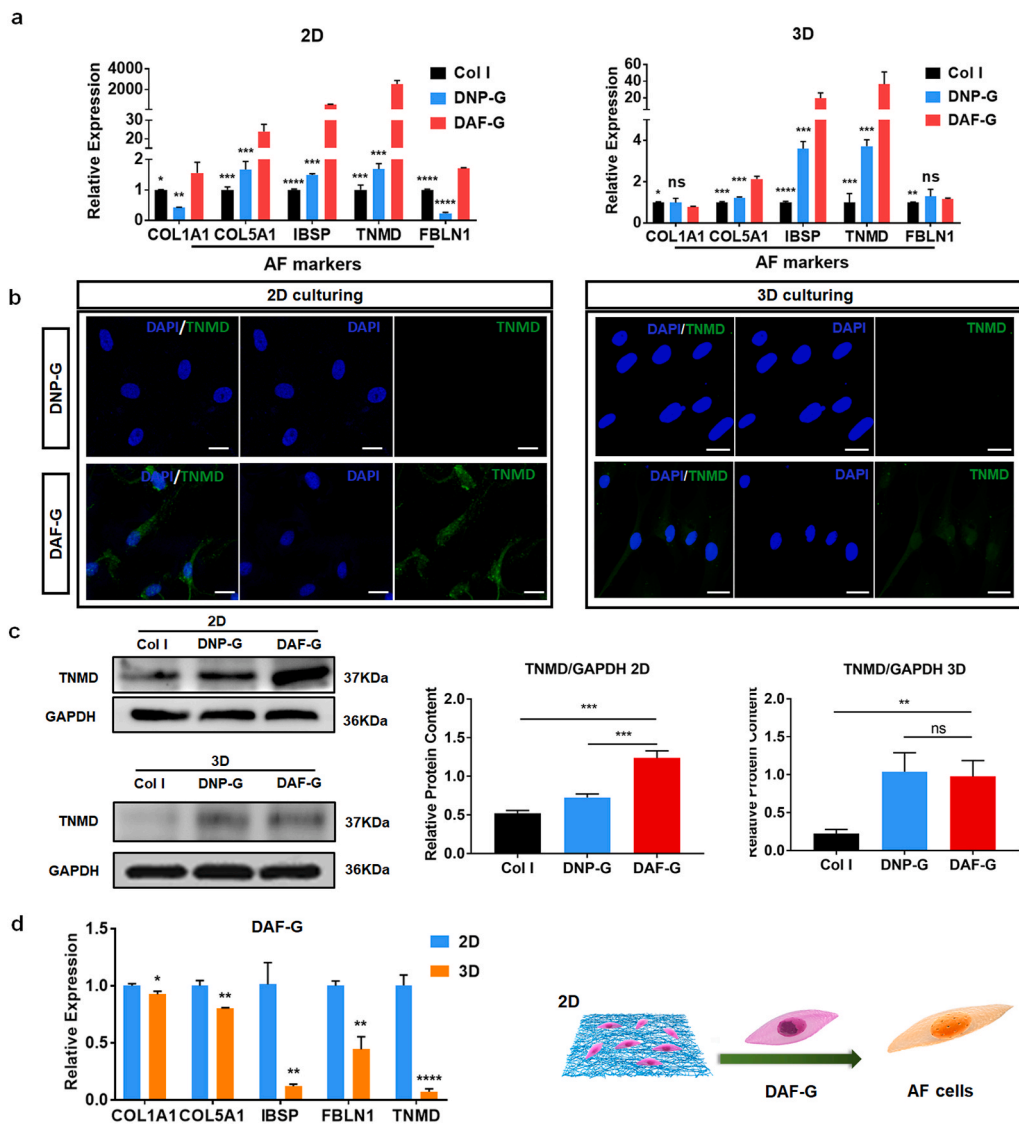


Fig. 4. Tissue-specific differentiation of hBMSCs towards AF like cells induced by DAF-G through component and spatial specificity. **a** RT-qPCR of AF-specific markers expressed in hBMSCs cultured in Col I, DNP-G and DAF-G under 2D or 3D culture. (Data are presented as the mean \pm SD, $n = 3$, * $p < 0.05$, ** $p < 0.01$, *** $p < 0.001$, **** $p < 0.0001$ between DNP-G and other groups; ns, no significance.) **b** Immunofluorescence of TNMD in hBMSCs cultured on DNP-G and DAF-G under 2D or 3D microenvironment. (Scale bar = 20 μ m) **c** Western blots and grayscale analysis of TNMD. **d** Differential expression of AF-specific markers in hBMSCs between 2D and 3D microenvironments. **e** Tissue-specific differentiation of hBMSCs towards AF cells was more likely achieved by DAF-G under 2D microenvironment. (Data are presented as the mean \pm SD, $n = 3$, * $p < 0.05$, ** $p < 0.01$, *** $p < 0.001$, **** $p < 0.0001$ between two groups; ns, no significance.)

transduces mechanical signals from the tissue architecture and surrounding ECM to an intercellular receptor to alter cellular activities [35]. However, its role in DNP-G- and DAF-G-related tissue and spatial specificity has not been identified. Therefore, we evaluated the adhesive property of cells in DNP-G 3D culturing and in DAF-G 2D culturing, after seeding hBMSCs on DTM for 21 days. Interestingly, compared with DNP-G 3D culturing, hBMSCs showed an enlarged cellular area on the DAF-G surface, with a larger focal adhesion area, indicating markedly enhanced cellular adhesion induced by DAF-G 2D culturing (Fig. 5a–b). Next, we evaluated the physical signaling sensor, the integrin family, and identified significant upregulated integrin α v β 3 in DAF-G 2D (Fig. 5c). Downstream RhoA activity was mostly enhanced in DAF-G 2D (Fig. 5c). Rho-GTPases functioned in YAP1 activation through the dephosphorylation of LATS1/2 [36]. Additionally, LATS phosphorylation was significantly reduced in DAF-G 2D, indicating inactivation of Hippo signaling (Fig. 5d). Consequently, YAP1 phosphorylation was downregulated, with decreased YAP1 degradation in DAF-G 2D (Fig. 5d). These results suggested that the integrin-mediated RhoA/LATS signaling pathway was differently altered in DNP-G 3D and DAF-G 2D, resulting in different YAP1 activity.

2.4. Opposite regulatory effects of YAP1 on tissue-specific hBMSCs differentiation induced by DNP-G and DAF-G

In the 3D culture condition, significant phosphorylation, and the transfer of YAP1 from the nucleus to the cytoplasm was observed in DNP-G (Fig. 6a–c), accompanied by the downregulation of its target proteins, including AREG, CYR61 and CTGF (Supplementary Fig. 3). To further identify the primary role of YAP1 in NP-like differentiation, the specific YAP1 inhibitor verteporfin was employed. Verteporfin (10 μ M) was efficient in inhibiting YAP1 and did not significantly impair cell viability (Supplementary Fig. 4). The addition of verteporfin also showed significantly higher GPC3 expression than the DMSO group tested by immunoblotting (Fig. 6d, Supplementary Fig. 5a–b). Generally, verteporfin significantly elevated the expression of NP-specific markers (Fig. 6e, Supplementary Fig. 5c). These results implied that YAP1 inhibition promoted the differentiation of cultured hBMSCs towards NP-like cells. Next, Lenti-YAP1 transfection was utilized to overexpress YAP1 (Supplementary Fig. 6a). Fluorescence staining indicated less obvious GPC3 accumulation in the Lenti-YAP1 group in DNP-G (Fig. 6f). Similarly, NP-specific markers expression was attenuated in DNP-G after YAP1 overexpression (Fig. 6g; Supplementary Fig. 6b). Furthermore, YAP1 overexpression significantly diminished GPC3 protein levels (Supplementary Fig. 6c–e). Therefore, the phosphorylation and

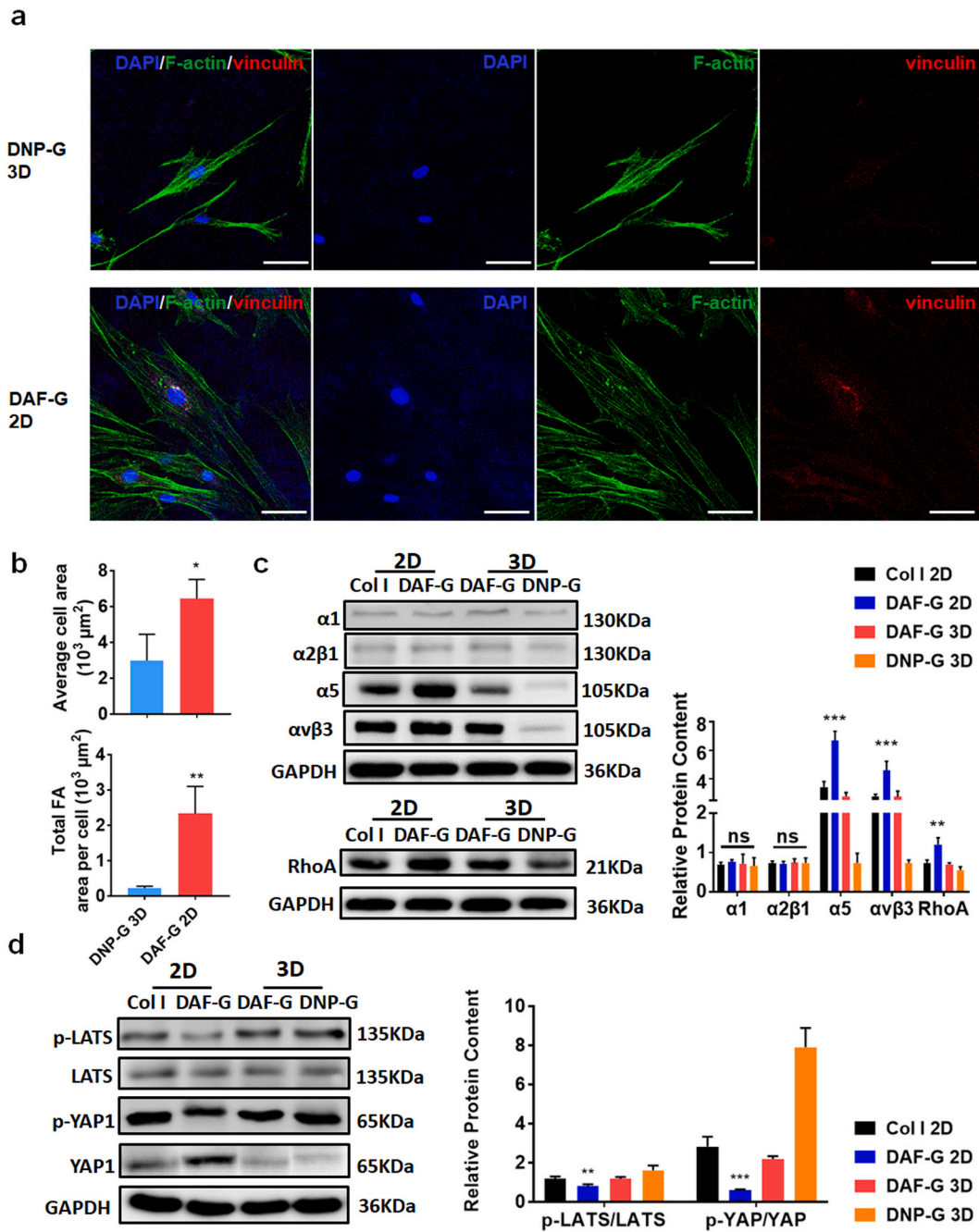
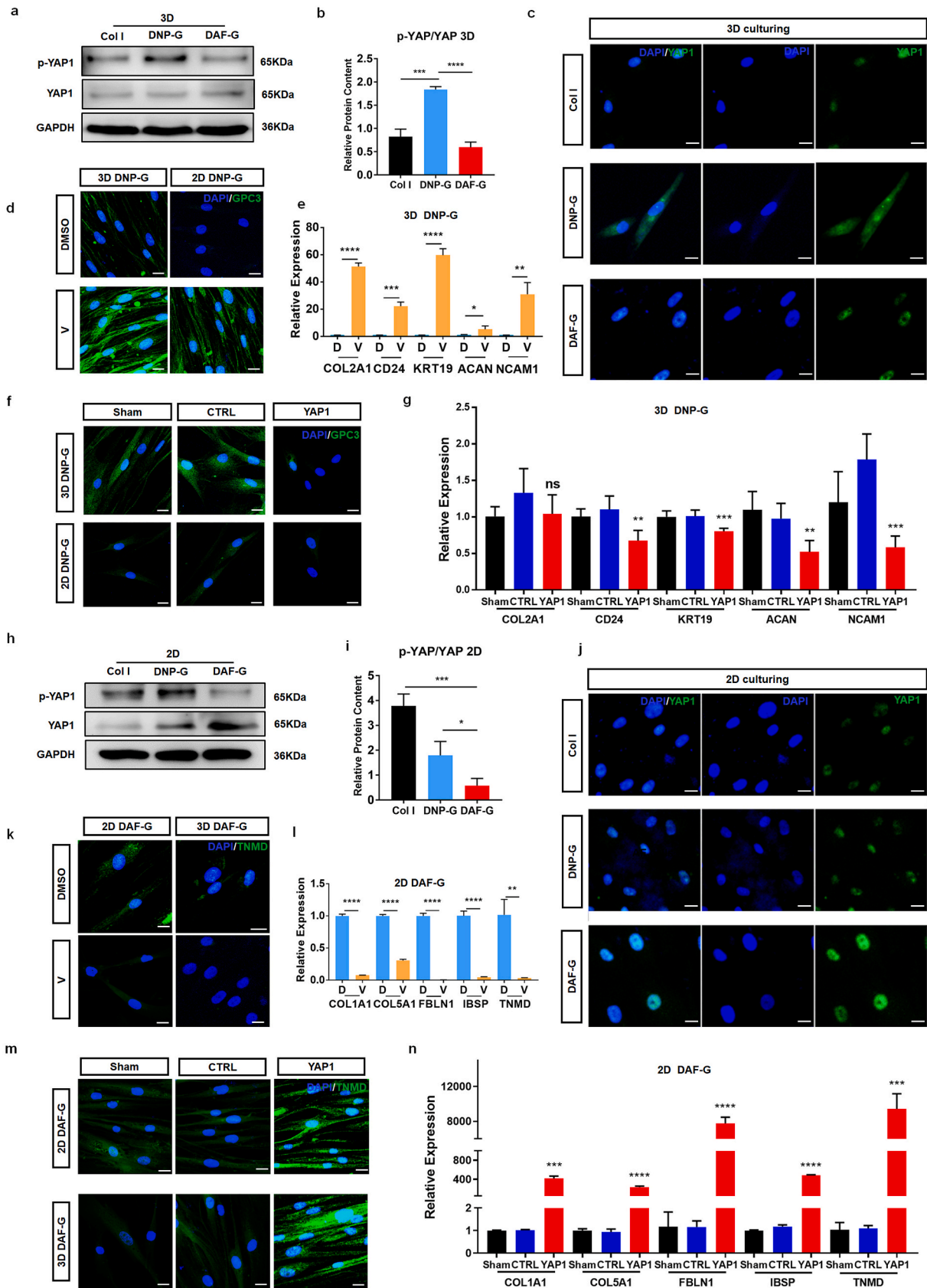


Fig. 5. Integrin $\alpha\beta 3$ /RhoA/LATS/YAP1 signaling acts in DTM-induced tissue-specific differentiation. **a** Immunofluorescence images of F-actin (green), vinculin (red) and DAPI (blue) in DNP-G under 3D microenvironment and DAF-G under 2D microenvironment. (Scale bar = 50 μm). **b** Quantitative analysis of average cellular area and focal adhesion area. (Data are presented as the mean \pm SD, $n = 3$, * $p < 0.05$, ** $p < 0.01$, *** $p < 0.001$, **** $p < 0.0001$ between two groups) **c** Integrin expression profile and RhoA activity in DTM. **d-e** Evaluation of LATS/YAP1 activation by Western blot. (Data are presented as the mean \pm SD, $n = 3$, ** $p < 0.01$, *** $p < 0.001$ between DAF-G 2D and DNP-G 3D; ns, no significance among groups.). (For interpretation of the references to colour in this figure legend, the reader is referred to the Web version of this article.)

cytoplasmic transfer of YAP1 promoted the differentiation of hBMSCs towards NP-like cells. These results suggest that YAP1 negatively regulates the NP-like differentiation of hBMSCs in DNP-G 3D culture.

Additionally, YAP1 expression in DAF-G showed the highest level among the three groups and was expressed in the nuclei with 2D culturing; however, p-YAP1 expression was less than that in the DNP-G group (Fig. 6h–j). The transcript levels of AREG, CYR61 and CTGF were also elevated in the DAF-G group (Supplementary Fig. 3). To further identify the regulatory role of YAP1 in AF-like differentiation, western blotting and RT-qPCR analysis after verteporfin treatment revealed that

the TNMD protein level was downregulated (Fig. 6k; Supplementary Figs. 5a–b), followed by downregulation of the COL1A1, COL5A1, IBSP, FBLN1 and TNMD levels (Fig. 6l; Supplementary Fig. 5d). These results implied that YAP1 inhibition might prohibit the differentiation of hBMSCs towards AF-like cells. Furthermore, Lenti-YAP1 transfection significantly upregulated the AF-specific markers on DAF-G (Fig. 6m–n; Supplementary Fig. 6d). YAP1 overexpression also upregulated the TNMD protein levels (Supplementary Fig. 6c–e). Therefore, upregulation and nuclear assembly of YAP1 led to the differentiation of hBMSCs into AF-like cells.



(caption on next page)

Fig. 6. Opposite regulatory effects of YAP1 on NP and AF-specific differentiation of hBMSCs. **a** p-YAP1 was enhanced in DNP-G under 3D microenvironment, with no significant difference for YAP1. **b** Statistical assessment of the p-YAP1/YAP1 protein content of each group. **c** Immunofluorescence of YAP1 showed that DNP-G in the 3D environment showed obvious YAP1 cytoplasmic gathering. **d** Immunofluorescence images showed that GPC3 protein was obviously upregulated by verteporfin in either 2D or 3D microenvironment. **e** NP-specific markers were all upregulated with verteporfin administration. **f** YAP1 overexpression diminished GPC3 protein expression. **g** YAP1 overexpression also diminished other NP-specific markers expression. **h** YAP1 protein expression was significantly enhanced in DAF-G, with less YAP1 phosphorylation. **i** Statistical assessment of the p-YAP1/YAP1 protein content of each group. **j** YAP1 nuclear assembly was significantly enhanced in DAF-G in the 2D environment. **k** AF-specific marker TNMD protein level was decreased with the administration of verteporfin. **l** verteporfin administration downregulated AF-specific markers. **m** YAP1 overexpression promoted TNMD protein expression and **n** other AF-specific markers expression on DAF-G. (scale bar = 20 μm) (Data are presented as the mean ± SD, n = 3, *p < 0.05, **p < 0.01, ***p < 0.001, ****p < 0.0001 between two groups; ns, no significance.) D, DMSO; V, verteporfin.

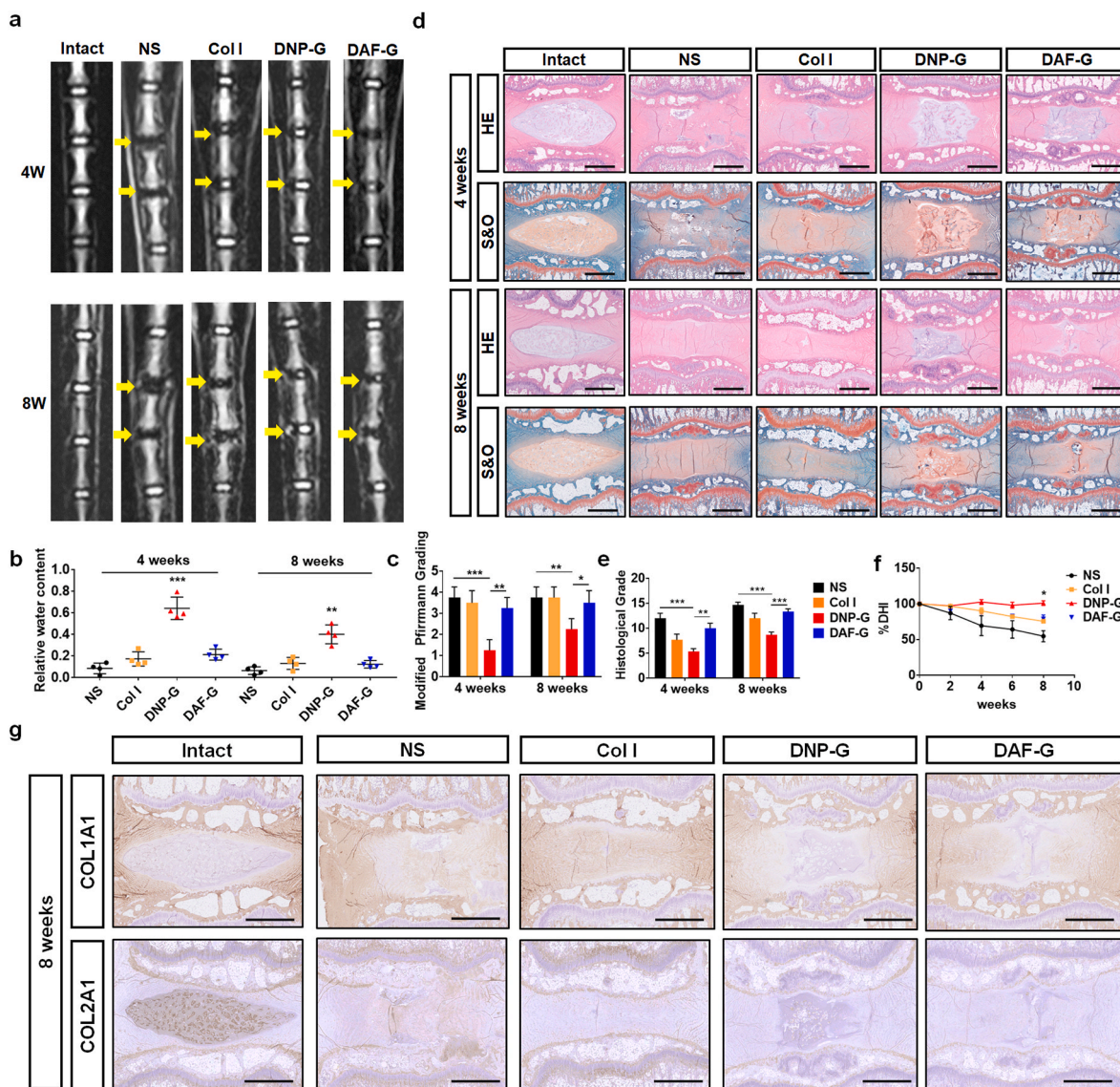


Fig. 7. The tissue-specific repair of NP tissues induced by DNP-G. **a** 4-week and 8-week T2-weighted images of rat tails injected with NS, Col I, DNP-G or DAF-G (yellow arrows point at the operated discs). **b** Relative water content and **c** modified Pfirrmann grades are presented to quantitatively assess disc degeneration based on MRI images. Assessment of disc degeneration in each group by **d** histological imaging and **e** grade (scale bar = 1 mm). **f** X-ray shows that the disc height is better preserved in the NP group than in the other groups. (Data are presented as the mean ± SD, n = 5, *p < 0.05, **p < 0.01, ***p < 0.001, ****p < 0.0001 between two groups; ns, no significance.) **g** Immunohistochemical staining of COL1A1 and COL2A1 (scale bar = 1 mm). (For interpretation of the references to colour in this figure legend, the reader is referred to the Web version of this article.)

2.5. Tissue-specific repair using DNP-G and DAF-G in vivo

To evaluate whether DNP-G was preferred to treat NP degeneration disease, different hydrogels were injected into the lesion site of an NP degeneration rat model. The improvement degree of injured NP tissue was compared via pathological and morphological analyses, 4 and 8 weeks post-surgery, respectively. As illustrated in MRI T2 phase images

(Fig. 7a), the NP integrity and water content were better preserved in the DNP-G group than in the other groups. Quantitation of the water content and modified Pfirrmann grading also revealed that the DNP-G group had the best recovery effects among all the treatment groups (Fig. 7b–c). Additionally, H&E and S&O staining showed that the NP tissues in the NS group were shrunken and irregularly shaped. By contrast, injection of DNP-G significantly alleviated the morphological aggravation of the NP

tissues at both predetermined time points (Fig. 7d). The rank of histological scoring from high to low was NS group > DAF-G group > Col I group > DNP-G group (Fig. 7e). Consistently with the MRI results, the % DHI drawn from X-ray showed that the disc heights in the DNP-G group were significantly larger than those in the NS, Col I and DAF-G groups 8 weeks post-surgery. Additionally, DNP-G significantly attenuated the aggravation of intervertebral disc narrowing (Fig. 7f; Supplementary Fig. 7a). IHC staining of COL1A1 and COL2A1 showed that the positive area for COL2A1 was significantly larger in DNP-G group than that in NS, Col I and DAF-G group at 8-week (Fig. 7g). COL1A1, a major fiber component of AF, indicated that the collagen fibers were more aligned in DNP-G group than that in other groups (Fig. 7g). Thus, these results suggested that the supplementation of NP-derived DTM hydrogel efficiently prevented NP degeneration.

Regarding the AF defect model, MRI showed that the DAF-G group exhibited the highest T2-weighted signal and water content but the lowest Pfirrmann score compared with the other three groups (Supplementary Figs. 7b–d), indicating that disc degeneration was significantly

delayed after administering DAF-G. H&E and S&O staining in the Col I gel and NS groups showed a sparse number of surviving cells in the NP tissues, accompanied by a low proteoglycan content and irregular ECM distribution. However, this degenerative morphology was considerably reversed in the DNP-G and DAF-G groups 4 weeks after treatment (Fig. 8a). Although the intervertebral discs in the NS group were further degenerated 12 weeks post-injury, the degeneration was greatly alleviated after administering DNP-G and DAF-G, particularly the latter. Furthermore, the residual AF collagen in the DAF-G group was well aligned (Fig. 8a). Additionally, COL1A1 staining showed that the annulus defect was still obvious in DNP-G and NS group compared with DAF-G group at 12-week, suggesting a well integration of DAF-G with surrounding tissues. Also, the positive area for COL2A1 was significantly larger in DAF-G group than that in NS, Col I and DNP-G group at 12-week (Fig. 8b). Quantitative histological grading showed that disc disruption was markedly repaired in the DAF-G group (Supplementary Fig. 7e). X-ray analysis also showed that the decline in the % DHI was slower in the DAF-G group than in either the DNP-G or Col I group

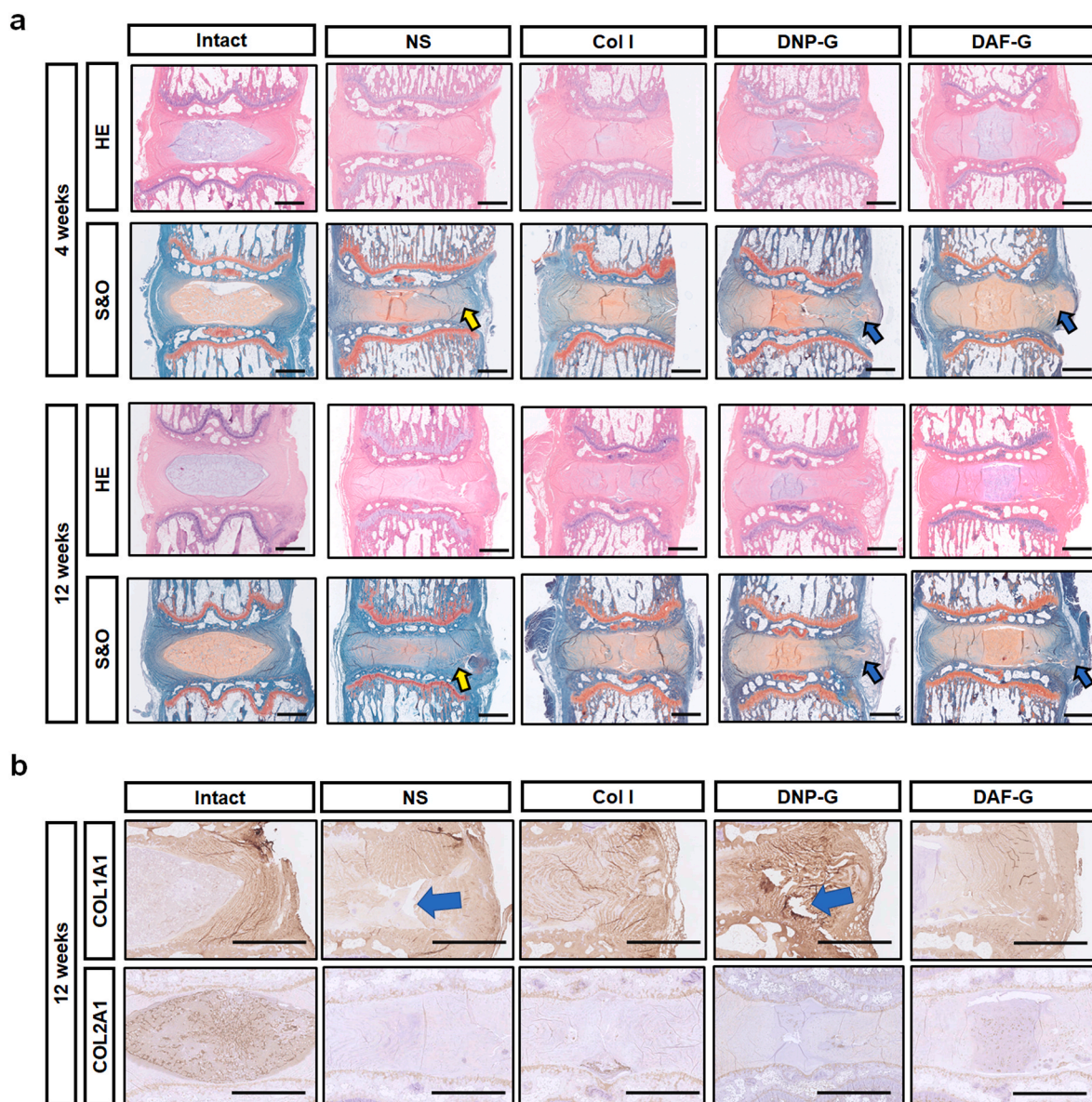


Fig. 8. The tissue-specific repair of AF tissues induced by DAF-G. **a** Representative HE and S&O staining were evaluated at 4 and 12 weeks in each group. Yellow arrows indicate the needle passage in the NS groups, and blue arrows indicate the inserted hydrogels. **b** Immunohistochemical staining of COL1A1 and COL2A1 (scale bar = 1 mm). (For interpretation of the references to colour in this figure legend, the reader is referred to the Web version of this article.)

(Supplementary Figs. 7f–g). Overall, these results demonstrated that the tissue-specific DTM hydrogels effectively repaired their corresponding tissue damage/defect in vivo.

3. Discussion

DTM materials derived from different tissues have shown substantial discrepancy in the manipulation of cellular behaviors. According to some pioneer reports [24,25,37], the original tissue or organ of specific DTM may determine multipotent stem cell differentiation and exhibit tissue regeneration capacity. This prompts the development of tissue-specific DTM biomaterials. In intervertebral discs, healthy NP mainly comprises entangled collagen type II fibers and a large amount of proteoglycan, which forms a highly hydrated structure [28]. AF is a well-organized lamellar structure filled with oriented collagen I fibers [27]. Inspired by the different structures and compositions of NP and AF, we speculate that DTM hydrogels derived from NP and AF may retain their biological functions of the native tissues, which may be mainly reflected in directing the differentiation of stem cells and in repairing their corresponding degenerated tissues.

Although several studies have investigated biomaterial-induced NP or AF cell-like differentiation [38,39], no standard molecules were identified to mark the NP or AF cell type. COL2A1 and ACAN were established as NP markers [40,41]. Additionally, CD24, KRT19 and GPC3 were recently recognized as NP-specific markers via microarrays and RT-qPCR [42–44]. Furthermore, NCAM1 was confirmed to be a human NP-specific marker by RT-qPCR analysis [43]. Therefore, COL2A1, CD24, KRT19, ACAN, NCAM1 and GPC3 were further verified in this study and served as NP-specific markers. Regarding AF differentiated molecules, Col 1a1 is the most broadly used gene marker of AF cells because collagen I is the primary component in AF tissues [40]. Other reports have recommended COL5A1 as a potential AF marker based on large-scale statistics [42,45]. In addition to the above AF markers, recent transcriptional profiling based on human intervertebral discs reported that IBSP, TNMD and FBLN1 showed higher expression levels in human AF cells than in NP cells [46]. Furthermore, in mature AF cells, we verified high expression of COL1A1, COL5A1, IBSP, FBLN1 and TNMD, which could serve as potential markers for AF cells.

Using the above-mentioned markers, the differentiation of hBMSCs induced by the type of hydrogel species or culture model was evaluated in detail. DNP-G induced hBMSCs to differentiate towards the NP-like cell type without any additional cytokines, particularly in the 3D hydrogel encapsulated model. Using proteomic analysis, we speculated that the cause might be related to FGF18 found in DNP-G. FGF18 promotes chondrogenic differentiation by upregulating ACAN and COL2A1 expression [47]. In addition to the diversity of growth factors, DNP-G contained abundant collagen, including COL2A1, COL11A2 and COL9A3. Collagen II promoted MSC differentiation into the NP-like cell type [48]. Additionally, healthy NP tissue is highly hydrated and NP cells are encapsulated in the gel-like microenvironment during intervertebral disc development [49]. Therefore, the 3D encapsulated culture model is potentially more favorable for hBMSCs differentiation into NP-like cells and can be extended to other biomaterials [50,51].

Similarly, DAF-G showed a greater potential in directing hBMSCs differentiation into AF-like cells, particularly those on the surface of hydrogels. We also found that TGF- β 1 only existed in DAF-G and was an efficient factor that maintained the AF-like cell type [15], although it might also induce NP-like differentiation [52]. Collagen I, mostly found in DAF-G, promoted the AF cell-like differentiation of MSCs [48]. Additionally, native AF tissue comprises 15 to 25 concentric rings in the lamellae structure with an AF cell interlayer accommodation [53]. AF cells are then forced to live between layers in an elongated morphology, similar to being seeded on the surface of substrates [38]. When cultured on the surface of PECUU (poly (ether carbonate urethane)urea) with a higher elastic modulus for 21 days, rabbit adipose-derived stem cells (ADSCs) gradually showed high expression of collagen I but low

expression of collagen II and GAG, indicating that ADSCs were differentiated into AF-like cells [54]. Consistently, our findings also suggested that the 2D culture model allowed hBMSCs to adapt to a native lamellar structure and promote their differentiation into AF-like cells. Therefore, the tissue specificity that affects the differentiation of stem cells comprises two parts, a matrix component and the physical presentation of the cell in/on the matrix. To investigate the differentiation behavior of hBMSCs in the in vitro model, we must consider both the composites of DNP-G and DAF-G, as well as whether the culture model of the cells is consistent with that of the body.

Integrin is a functional adapter that transfers external physical stimulation into intracellular signaling [55]. Interestingly, different types of collagens and subtypes of integrin can interact to determine cell fate. For example, integrin α 2 β 1, α 1 β 1, α 5 β 1 on chondrocytes binds to the primary type II collagen and determines chondrocyte differentiation and joint formation [56,57]. Additionally, α 2 β 1, α 1 β 1, and α v β 3 are a major class of collagen-binding proteins that are activated in the cell-collagen type I interaction [58,59]. Therefore, we compared the activation of these integrins in four significantly different states, DAF-G 2D, DAF-G 3D and DNP-G 3D. We found that integrin α v β 3 was mostly upregulated in DAF-G 2D, while integrin α v β 3 in Col I 2D and DAF-G 3D also activated, compared with DNP-G 3D. Therefore, DAF-G 2D induced the activation of integrin α v β 3, which may be largely associated with the components and spatial characteristics. Additionally, integrin α v β 3 activation was reported to enhance collagen type I expression [60], which may favor differentiation into the AF cell type [38]. In response to integrin transformation, cytoskeleton-mediated Rho-GTPases act in YAP1 activation and dephosphorylation in a LATS1/2-dependent or LATS1/2-independent manner [61,62]. In our study, compared with cells in DNP-G in 3D, cells in DAF-G 2D showed a larger cellular area and more cell adhesion to ECM, activating the integrin family via mechanical signals [63,64]. Specifically, integrin α v β 3 was activated not only by the compositional difference but also by external physical stimulation in DAF-G 2D, inducing F-actin-related RhoA-GTPase promotion and resulting in LATS-mediated YAP1 dephosphorylation in DAF-G 2D. However, the mechanism of YAP1 deactivation in DNP-G 3D requires further investigation.

YAP1 is a fundamental transcription coactivator that not only regulates cell proliferation and differentiation [65] but also controls organ size [66] and tissue homeostasis [67]. This gene has also been proven to be associated with osteogenesis [68], and its nuclear assembly was related to direct AF-like differentiation [38]. In this study, we also detected elevated YAP1 nuclear aggregation and decreased YAP1 phosphorylation after culturing hBMSCs in a 2D DAF-G environment. More interestingly, hBMSCs showed a significantly high phosphorylation and cytoplasmic distribution of YAP1 when 3D cultured in DNP-G, suggesting that the activation or suppression of YAP1 was associated with the in vitro differentiation of hBMSCs into AF-like or NP-like cells. Previous reports have demonstrated that stem cells incubated in a 3D environment with low stiffness (less than 10 kPa) exhibited gradual YAP1 cytoplasmic gathering and dysfunction [69], which might be due to the absence of robust stress fibers in 3D substrates [70,71]. Other researchers found that MCF10A breast cancer cells showed significant YAP1 nuclear localization in 2D stiff polyacrylamide (PAM) [72]. Consistent with the literature, YAP1 localizes in the nucleus and exerts transcription effects on 2D stiff substrates, and cytoplasmic assembly is intended to appear within 3D and softer materials. Additionally, considering that the storage modulus of DAF-G was larger than that of DNP-G, YAP1 nuclear accumulation in DAF-G 2D may be attributed to both the culture dimensions and mechanical properties via the integrin/Rho/LATS1/2 signaling pathway. Moreover, Gel-HA with decreased mechanical strength showed increased expression of SOX9, ACAN and COL2A1, decreased COL1A1 [73]. Transcriptome RNA sequencing showed decreased mechanical strength was accompanied with YAP1 degradation, indicating that softer substance may increase NP phenotype, while inhibiting AF phenotype via YAP1 deactivation [73], which

is consistent to our findings in DNP-G.

Apart from the mechanical difference, DTM components differences may also influence YAP1 intracellular distribution. TGF- β 1, identified in DAF-G, was reported to mediate YAP1 activation via PI3K/Akt pathway, resulting in myofibroblasts phenotype [74,75]. YAP1 target gene subsets were also largely dependent on endogenous TGF- β 1 signaling [76]. Therefore, high expression of TGF- β 1 in DAF-G may also contribute to observed YAP1 activation in DAF-G 2D. The relationship between FGF-18 (found in DNP-G) and YAP1 has rarely been investigated. Another member of FGF families, FGF-2, was also found to promote chondrogenic lineages and related to YAP1 [77]. And YAP1 activation mediated by FGF is dose-dependent. FGF-2 of low concentration (5 ng/ml) was found to induce YAP1 nuclear localization [78], while higher concentration (200 ng/ml) showed activation of Hippo signaling and promoted YAP1 deactivation. Whether the differences in collagen types would contribute to YAP1 intracellular distribution requires further evaluation.

Furthermore, we found that the inhibition of YAP1 activation significantly diminished the AF-like cell type in DAF-G and promoted the NP-like cell type in DNP-G, while YAP1 overexpression exhibited opposite results. To our knowledge, these findings clarify the seesaw effects by which the activation level of YAP1 determines the fate of hBMSCs to differentiate into NP-like or AF-like cells, providing theoretical support for the future developments for IDD treatments using stem cell therapy.

From the *in vitro* assessments, we realized that the DTM biomaterials with closer biomimetic structure and biological activity to their native tissues provide a more permissive microenvironment for intervertebral disc cells, likely beneficial for better repair of their corresponding degenerated tissues. Therefore, the tissue specificity of both DNP-G and DAF-G was explored *in vivo*. Both the NP degenerative model and AF defect model were applied in this study according to previous studies [1, 79,80]. Intradiscal puncture-induced NP degeneration led to an unfavorable microenvironment because of poor nutrient and oxygen support, low pH, anabolism, and catabolism imbalance. Thus, this model can sufficiently imitate the native ongoing NP degeneration. However, the annular defects often lead to gaps in AF tissue and induce herniation of NP tissue under intradiscal pressure, which mimics the pathophysiological change in the intervertebral disc after minor AF trauma [81]. In the present study, after the injection of DNP-G, DAF-G or Col I hydrogel into the defects, DNP-G was more favorable for restoring NP degeneration than the other groups, while DAF-G showed superior capability in repairing annular defects and maintaining NP tissues. During the pathogenesis of disc degeneration, disorders of intercellular and cell-ECM interactions are commonly noticed because of the aberrant assembly of GAG [82], catabolism of collagen type II and anabolism of collagen type I in NP [4]. Coincidentally, our results from GAG quantitation and proteomic analysis showed that DNP-G possesses more GAG and collagen type II contents, but less collagen type I than that of DAF-G. These abundant components in the DNP-G may contribute to restore the cell-ECM interactions, promoting the regeneration of NP tissue. TGF- β 1, which has been verified to restrain cell apoptosis [83], was only detected in DAF-G. Moreover, DAF-G retained more collagen type I but less collagen type II than DNP-G. These results indicated that the compositional similarity of the native tissues and DTM materials would be suitable to treat their corresponding diseases, such as the use of cornea-derived decellularized ECM for corneal regeneration [84] and the triphasic decellularized bone-fibrocartilage-tendon (D-BFT) composite scaffold for enthesis regeneration [85], because of the tissue-specific biochemical and mechanically stable microenvironment for controlling specific cellular behaviors [86].

There are some limitations in the present study. First, DNP-G and DAF-G possess poor mechanical properties that cannot compete with the strength of natural NP and AF tissues. Thus, we will enhance their mechanical properties while exploiting its unique biological effects in future studies. Second, to assess the tissue specificity of the *in vivo* repair

effect of DNP-G and DAF-G, stem cell delivery was not performed for *in vivo* repair; thus, the underlying regulation mechanism of specific differentiation was not verified *in vivo*. Finally, although the regulatory relationship between collagen type I and integrins has been reported [58,59], chemical-related, tissue-specific differentiation towards AF cells cannot be simply attributed to collagen type I because DAF-G 2D showed higher activation of integrin α v β 3 and better promoted the AF cell phenotype than collagen type I. Thus, other components that contribute to tissue-specific differentiation should be further identified. Additionally, the characteristics that inhibit YAP1 activation in DNP-G 3D should be further investigated to better understand the regulatory effects of YAP1 and provide a theoretical basis for promoting the application of DTM.

In summary, this original study demonstrates that the tissue specificity of DNP-G and DAF-G for specific differentiation towards NP or AF cells relies on both ECM components and spatial characteristics. The regulation of the integrin-mediated RhoA/LATS/YAP1 signaling pathway determines the fate of hBMSCs. Importantly, the tissue-specific regeneration of DNP-G and DAF-G for the NP degenerative model and AF defect model, respectively, was also identified. Because of the plasticity of hydrogels, 3D bioprinting, electrospinning, phase separation and other processing methods can be further performed to construct the spatial architectures of NP and AF, as well as maintain their functional ECM components, providing efficient therapeutic strategies to repair degenerated NP and AF tissues.

4. Materials and methods

4.1. Preparation of bovine outer annulus fibrosus and nucleus pulposus samples

All animal experiments were approved by the Animal Experimentation Committee of Huazhong University of Science and Technology and complied with institutional and international guidelines. Samples were collected from the caudal segments of bovine ($n = 30$) within 6 h of sacrifice. NP and AF tissues were isolated carefully from each sample, and were subjected to five freeze–thaw cycles. Cellular components in NP and AF samples were sequentially decellularized by Triton X-100 (2%), sodium dodecyl sulfate (SDS, 1%) and DNAase (Sigma, 200 U/ml in PBS). The decellularized NP (DNP) and AF (DAF) samples were then washed in sterile water. Freeze-drying processes were then performed and the lyophilized decellularized tissues were homogenized into DNP powder or DAF powder. Decellularized matrix hydrogels were prepared as previously described [16]. Specifically, a certain amount of sterilized DTM powder was added into 0.01 M hydrochloric acid containing pepsin (concentration of pepsin is 1.5 mg/ml) to adjust its concentration to 10 mg/ml. After moderate agitation at 25 °C for 24–48 h, the pH of the digested solution was adjusted to 7.3–7.5 with 0.1 mol/l NaOH and the ionic strength was adjusted to 0.15 M using 10 × Phosphate-Buffered Saline (PBS; 1/10 of final neutralized volume). Finally, the DTM hydrogel was obtained after incubation at 37 °C for 10–30 min.

4.2. Cell removal and glycosaminoglycans maintenance after decellularization

To evaluate the degree of decellularization, the residual DNA in lyophilized native tissue or decellularized tissues was quantified by DNeasy assay, tissue hematoxylin and eosin (H&E) staining and 4',6-diamidino-2-phenylindole (DAPI, Beyotime, China) staining. The glycosaminoglycans (GAGs) content in decellularized tissues were assessed via quantifying the amount of sulfated glycosaminoglycans by 1,9-dimethylmethylene blue solution (GENMED, China) according to the manufacturer's instructions. The total collagen content of materials was measured by quantifying the amount of hydroxyproline with a kit (KGT030-2, keyGEN BioTECH, Nanjing, China), as previously described [87]. A hydroxyproline (Sigma-Aldrich) standard curve was generated

to determine the hydroxyproline concentration. Total collagen content was calculated based on that Hydroxyproline content was assumed to be 13–14% of the total collagen content per dry weight [88].

4.3. Characterization of decellularized matrix hydrogels

The rheological properties of DNP-G and DAF-G were analyzed with a strain-controlled rheometer (Thermo Scientific, HAAKE MARS III, Germany). The shear frequency was set to 1 Hz and shear strain was set to 1%.

Fresh tissues, decellularized matrix and decellularized matrix hydrogel were prepared for SEM. All prepared samples were observed by SEM (HITACHI S-4800) at 10 kV. The structural parameters of samples were measured by image analysis software (Image J; National Institutes of Health).

4.4. Isolation and characterization of hBMSCs, NP cells and AF cells

All experimental protocols involving human tissue and cells were carried out following The Code of Ethics of the World Medical Association (Declaration of Helsinki) for experiments involving humans and approved by the medical ethics committee of Tongji Medical College of Huazhong University of Science and Technology, and the informed consent of all participating subjects was obtained. As previously described [16], hBMSCs were extracted from the bone marrow in artificial hip joint replacements. The stemness was evaluated by cellular markers (anti-CD73-APC, anti-CD90-APC, anti-CD105-APC, anti-34-APC, anti-CD45-APC, Biologend, USA) (Supplementary Fig. 8a) and the efficacy of osteogenic, chondrogenic and adipogenic differentiation kits (Corning, USA) (Supplementary Fig. 8b).

NP tissue and AF tissue were separated from patients with lumbar disc herniation through a microscope operation. The extract of NP cells was performed as previously described [89]. Similarly, AF tissue was cut into small pieces and completely immersed in 0.02% type I collagenase for digesting 2 h at 37 °C. Then, the suspension was centrifuged at 300 g for 5 min to collect AF cells. Subsequently, these primary cells were cultured with DMEM/F12 complete medium. To distinguish the NP cells from the AF cells, the transcript expressions of COL2A1, CD24, KRT19, ACAN, NCAM1, COL1A1, COL5A1, IBSP, FBLN1, TNMD were detected.

4.5. Real-time quantitative polymerase chain reaction (RT-qPCR) analysis

Total RNA was isolated using TRIzol® Reagent (Invitrogen). mRNA expression was detected by real-time PCR with all-in-One™ qPCR Master Mix (GeneCopoeia, USA) using the ABI stepone plus Sequence Detection System (Applied Biosystems, CA, USA). The primer sequences used for PCR were listed in Supplementary Table 1. Results were quantified using the $2^{-\Delta\Delta CT}$ method with GAPDH expression levels for normalization.

4.6. Protein extraction and western blot

Cells embedded in hydrogels or planted on hydrogels were collected and lysed in lysis buffer (Beyotime, Jiangsu, China) containing a mixture of protease inhibitors phenylmethanesulfonyl fluoride (PMSF, Beyotime) and phosphatase inhibitor cock-tail I (Sigma, USA). BCA Protein Assay Kit (Beyotime) was used to detect the protein concentration. Equivalent amounts of protein (20 µg) were loaded on 10% or 8% SDS-PAGE gels.

Western blot was performed as previously described [90]. The antibodies were listed as follows: Integrin $\alpha 1$ (1:1000, ABclonal, A16054), $\alpha 2\beta 1$ (1:1000, Abcam, ab24697), $\alpha 5$ (1:1000, ABclonal, A19069), $\alpha v\beta 3$ (1:1000, ABclonal, A0076), RhoA (1:1000, ABclonal, A13947), LATS (1:1000, ABclonal, A7159), LATS (phosphorylation S909, 1:1000, ABclonal, AP0879), YAP1 (1:1000, Abcam, ab52771), YAP1

(phosphorylation S127, 1:1000, Abcam, ab76252), TNMD (1:1000, ABclonal, A17753), GPC3 (1:1000, Abcam, ab66596), AREG (1:1000, ABclonal, A12680), CYR61 (1:1000, ABclonal, A1111), CTGF (1:1000, ABclonal, A11943) and GAPDH (1:2000, Abcam, ab181602).

4.7. Statistical analysis

All experiments were repeated at least three times. Data were expressed as means \pm standard deviation (SD). The statistical differences between treatment groups were evaluated by Student's t-test or one-way analysis of variance (ANOVA) based on data normality. Statistical analyses were performed using the SPSS software package (IBM SPSS software package 18.0). All the statistical chart was drawn by GraphPad Prism 7 software (GraphPad Software Inc., San Diego, CA). P values < 0.05 were considered statistically significant.

4.8. Other methods

Methods that applied for proteomic analysis, cells viability, construction of lentivirus and cell transfection, in vivo experiments and histological staining etc. are described in Supplementary materials.

Data availability

The authors declare that all data supporting the findings of this study are available within the paper and its supplementary information files.

CRedit authorship contribution statement

Yizhong Peng: contributed equally to the work and shall share the first authorship, performed the experiments and analyzed the data-composed the majority of the manuscript and art works, finished the revision. **Xiangcheng Qing:** contributed equally to the work and shall share the first authorship, performed the experiments and analyzed the data, composed the majority of the manuscript and art works, revised the manuscript. **Hui Lin:** contributed equally to the work and shall share the first authorship, performed the experiments and analyzed the data-composed the majority of the manuscript and art works. **Donghua Huang:** performed the experiments and analyzed the data. **Jinye Li:** revised the manuscript. **Shuo Tian:** provided technical assistant, revised the manuscript, finished the revision. **Sheng Liu:** performed the experiments and analyzed the data. **Xiao Lv:** provided technical assistant. **Kaige Ma:** reviewed the final draft and approved the manuscript. **Rui Li:** composed the majority of the manuscript and art works. **Zilong Rao:** performed the experiments and analyzed the data. **Ying Bai:** revised the manuscript. **Songfeng Chen:** provided technical assistant. **Ming Lei:** supervised the process of experiments, manuscript drafting and determined the final draft. **Daping Quan:** designed the study and provided financial support, revised the manuscript. **Zengwu Shao:** designed the study and provided financial support, supervised the process of experiments, manuscript drafting and determined the final draft, All authors reviewed the final draft and approved the manuscript.

Declaration of competing interest

The authors declare no conflict of interest.

Acknowledgements

This work was supported by the Major Research Plan of National Natural Science Foundation of China [No.91649204], the National Key Research and Development Program of China [2016YFC1100100], the Scientific Research Training Program for Young Talents from Union Hospital, Tongji Medical College, Huazhong University of Science and Technology, National Natural Science Foundation of China (82002333). These fundings were not involved in the collection, analysis, or

interpretation of data in the study.

Appendix A. Supplementary data

Supplementary data to this article can be found online at <https://doi.org/10.1016/j.bioactmat.2021.03.014>.

References

- [1] Y. Moriguchi, B. Borde, C. Berlin, C. Wipplinger, S.R. Sloan, S. Kirnaz, B. Pennicooke, R. Navarro-Ramirez, T. Khair, P. Grunert, E. Kim, L. Bonassar, R. Hartl, In vivo annular repair using high-density collagen gel seeded with annulus fibrosus cells, *Acta Biomater.* 79 (2018) 230–238, <https://doi.org/10.1016/j.actbio.2018.07.008>.
- [2] W. Tong, Z. Lu, L. Qin, R.L. Mauck, H.E. Smith, L.J. Smith, N.R. Malhotra, M. F. Heyworth, F. Caldera, M. Enomoto-Iwamoto, Y. Zhang, Cell therapy for the degenerating intervertebral disc, *Transl. Res.* 181 (2017) 49–58, <https://doi.org/10.1016/j.trsl.2016.11.008>.
- [3] A. Hensley, J. Rames, V. Casler, C. Rood, J. Walters, C. Fernandez, S. Gill, J. J. Mercuri, Decellularization and characterization of a whole intervertebral disk xenograft scaffold, *J. Biomed. Mater. Res. A* 106 (2018) 2412–2423, <https://doi.org/10.1002/jbm.a.36434>.
- [4] Y.J. Chuah, Y. Peck, J.E.J. Lau, H.T. Hee, D.-A. Wang, Hydrogel based cartilaginous tissue regeneration: recent insights and technologies, *Biomater. Sci.* 5 (2017) 613–631, <https://doi.org/10.1039/c6bm00863a>.
- [5] R.D. Bowles, L.A. Setton, Biomaterials for intervertebral disc regeneration and repair, *Biomaterials* 129 (2017) 54–67, <https://doi.org/10.1016/j.biomaterials.2017.03.013>.
- [6] T.C. Schmitz, E. Salzer, J.F. Crispin, G.T. Fabra, C. LeVisage, A. Pandit, M. Tryfonidou, C. Le Maitre, K. Ito, Characterization of biomaterials intended for use in the nucleus pulposus of degenerated intervertebral discs, *Acta Biomater.* 114 (2020) 1–15, <https://doi.org/10.1016/j.actbio.2020.08.001>.
- [7] C.J. Panebianco, J.H. Meyers, J. Gansau, W.W. Hom, J.C. Iatridis, Balancing biological and biomechanical performance in intervertebral disc repair: a systematic review of injectable cell delivery biomaterials, *Eur. Cell. Mater.* 40 (2020) 239–258, <https://doi.org/10.22203/eCM.v040a15>.
- [8] C. Borrelli, C.T. Buckley, Injectable disc-derived ECM hydrogel functionalised with chondroitin sulfate for intervertebral disc regeneration, *Acta Biomater.* 117 (2020) 142–155, <https://doi.org/10.1016/j.actbio.2020.10.002>.
- [9] H. Xu, M. Sun, C. Wang, K. Xia, S. Xiao, Y. Wang, L. Ying, C. Yu, Q. Yang, Y. He, A. Liu, L. Chen, GDF5-GelMA injectable microspheres laden with adipose-derived stem cells for disc degeneration repair, *Biofabrication* (2020), <https://doi.org/10.1088/1758-5090/abc4d3>.
- [10] G. Feng, Z. Zhang, M. Dang, K.J. Rambahia, P.X. Ma, Nanofibrous spongy microspheres to deliver rabbit mesenchymal stem cells and anti-miR-199a to regenerate nucleus pulposus and prevent calcification, *Biomaterials* 256 (2020) 120213, <https://doi.org/10.1016/j.biomaterials.2020.120213>.
- [11] K. Prudnikova, S.E. Lightfoot Vidal, S. Sarkar, T. Yu, R.W. Yucha, N. Ganesh, L. S. Penn, L. Han, C.L. Schauer, E.J. Vresilovic, M.S. Marcolongo, Aggrecan-like biomimetic proteoglycans (BPGs) composed of natural chondroitin sulfate bristles grafted onto a poly(acrylic acid) core for molecular engineering of the extracellular matrix, *Acta Biomater.* 75 (2018) 93–104, <https://doi.org/10.1016/j.actbio.2018.05.013>.
- [12] U.Y. Choi, H.P. Joshi, S. Payne, K.T. Kim, J.W. Kyung, H. Choi, M.J. Cooke, S. Y. Kwon, E.J. Roh, S. Sohn, M.S. Shoichet, I. Han, An injectable hyaluronan-methylcellulose (HAMC) hydrogel combined with wharton's jelly-derived mesenchymal stromal cells (WJ-MSCs) promotes degenerative disc repair, *Int. J. Mol. Sci.* 21 (2020), <https://doi.org/10.3390/ijms21197391>.
- [13] C. Cunha, G.Q. Teixeira, C. Ribeiro-Machado, C. L. Pereira, J.R. Ferreira, M. Molinos, S. G Santos, M.A. Barbosa, R.M. Goncalves, Modulation of the in vivo inflammatory response by pro- versus anti-inflammatory intervertebral disc treatments, *Int. J. Mol. Sci.* 21 (2020), <https://doi.org/10.3390/ijms21051730>.
- [14] E. Durdag, O. Ayden, S. Albayrak, I.B. Atci, E. Armagan, Fragmentation to epidural space: first documented complication of Gelstix(TM.), *Turk. Neurosurg.* 24 (2014) 602–605, <https://doi.org/10.5137/1019-5149.JTN.9328-13.1>.
- [15] J. Du, R.G. Long, T. Nakai, D. Sakai, L.M. Benneker, G. Zhou, B. Li, D. Eglin, J. C. Iatridis, M. Alini, S. Grad, Z. Li, Functional cell phenotype induction with TGF-beta1 and collagen-polyurethane scaffold for annulus fibrosus rupture repair, *Eur. Cell. Mater.* 39 (2020) 1–17, <https://doi.org/10.22203/eCM.v039a01>.
- [16] Y. Peng, D. Huang, J. Li, S. Liu, X. Qing, Z. Shao, Genipin-crosslinked decellularized annulus fibrosus hydrogels induces tissue-specific differentiation of bone mesenchymal stem cells and intervertebral disc regeneration, *J. Tissue Eng. Regen. Med.* 14 (2020) 497–509, <https://doi.org/10.1002/term.3014>.
- [17] R. Kang, H. Li, Z. Xi, S. Ringgard, A. Baatrup, K. Rickers, M. Sun, D.Q.S. Le, M. Wang, L. Xie, Y. Xie, M. Chen, C. Bünger, Surgical repair of annulus defect with biomimetic multilamellar nano/microfibrous scaffold in a porcine model, *J. Tissue Eng. Regen. Med.* 12 (2018) 164–174, <https://doi.org/10.1002/term.2384>.
- [18] D. Sakai, G.B.J. Andersson, Stem cell therapy for intervertebral disc regeneration: obstacles and solutions, *Nat. Rev. Rheumatol.* 11 (2015) 243–256, <https://doi.org/10.1038/nrrheum.2015.13>.
- [19] G. Vadalà, L. Ambrosio, F. Russo, R. Papalia, V. Denaro, Interaction between mesenchymal stem cells and intervertebral disc microenvironment: from cell therapy to tissue engineering, *Stem Cell. Int.* 2019 (2019) 2376172, <https://doi.org/10.1155/2019/2376172>.
- [20] D.C. Noriega, F. Ardura, R. Hernandez-Ramajo, M.A. Martin-Ferrero, I. Sanchez-Lite, B. Toribio, M. Alberca, V. Garcia, J.M. Moraleda, A. Sanchez, J. Garcia-Sancho, Intervertebral disc repair by allogeneic mesenchymal bone marrow cells: a randomized controlled trial, *Transplantation* 101 (2017) 1945–1951, <https://doi.org/10.1097/TP.0000000000001484>.
- [21] Y. Hu, L. Huang, M. Shen, Y. Liu, G. Liu, Y. Wu, F. Ding, K. Ma, W. Wang, Y. Zhang, Z. Shao, X. Cai, L. Xiong, Pioglitazone protects compression-mediated apoptosis in nucleus pulposus mesenchymal stem cells by suppressing oxidative stress, *Oxid. Med. Cell. Longev.* 2019 (2019) 4764071, <https://doi.org/10.1155/2019/4764071>.
- [22] W.-H. Chen, H.-Y. Liu, W.-C. Lo, S.-C. Wu, C.-H. Chi, H.-Y. Chang, S.-H. Hsiao, C.-H. Wu, W.-T. Chiu, B.-J. Chen, W.-P. Deng, Intervertebral disc regeneration in an ex vivo culture system using mesenchymal stem cells and platelet-rich plasma, *Biomaterials* 30 (2009) 5523–5533, <https://doi.org/10.1016/j.biomaterials.2009.07.019>.
- [23] L.T. Saldin, M.C. Cramer, S.S. Velankar, L.J. White, S.F. Badylak, Extracellular matrix hydrogels from decellularized tissues: structure and function, *Acta Biomater.* 49 (2017) 1–15, <https://doi.org/10.1016/j.actbio.2016.11.068>.
- [24] W. Han, N.K. Singh, J.J. Kim, H. Kim, B.S. Kim, J.Y. Park, J. Jang, D.-W. Cho, Directed differential behaviors of multipotent adult stem cells from decellularized tissue/organ extracellular matrix bioinks, *Biomaterials* 224 (2019) 119496, <https://doi.org/10.1016/j.biomaterials.2019.119496>.
- [25] B.B. Rothrauff, G. Yang, R.S. Tuan, Tissue-specific bioactivity of soluble tendon-derived and cartilage-derived extracellular matrices on adult mesenchymal stem cells, *Stem Cell Res. Ther.* 8 (2017) 133, <https://doi.org/10.1186/s13287-017-0580-8>.
- [26] Y. Xu, J. Zhou, C. Liu, S. Zhang, F. Gao, W. Guo, X. Sun, C. Zhang, H. Li, Z. Rao, S. Qiu, Q. Zhu, X. Liu, X. Guo, Z. Shao, Y. Bai, X. Zhang, D. Quan, Understanding the role of tissue-specific decellularized spinal cord matrix hydrogel for neural stem/progenitor cell microenvironment reconstruction and spinal cord injury, *Biomaterials* 268 (2020) 120596, <https://doi.org/10.1016/j.biomaterials.2020.120596>.
- [27] M. Gluais, J. Clouet, M. Fusellier, C. Decante, C. Moraru, M. Dutilleul, J. Veziere, J. Lesoeur, D. Dumas, J. Abadie, A. Hamel, E. Bord, S.Y. Chew, J. Guicheux, C. Le Visage, In vitro and in vivo evaluation of an electrospun-aligned microfibrillar implant for Annulus fibrosus repair, *Biomaterials* 205 (2019) 81–93, <https://doi.org/10.1016/j.biomaterials.2019.03.010>.
- [28] Z. Li, X. Li, C. Chen, M.T.V. Chan, W.K.K. Wu, J. Shen, Melatonin inhibits nucleus pulposus (NP) cell proliferation and extracellular matrix (ECM) remodeling via the melatonin membrane receptors mediated PI3K-Akt pathway, *J. Pineal Res.* 63 (2017), <https://doi.org/10.1111/jpi.12435>.
- [29] A.H. Aziz, R.L. Wilmoth, V.L. Ferguson, S.J. Bryant, IDG-SW3 osteocyte differentiation and bone extracellular matrix deposition are enhanced in a 3D matrix metalloproteinase-sensitive hydrogel, *ACS Appl. Bio Mater.* 3 (2020) 1666–1680, <https://doi.org/10.1021/acsabm.9b01227>.
- [30] S. Rumiński, I. Kalaszczynska, A. Dlugosz, M. Lewandowska-Szumiel, Osteogenic differentiation of human adipose-derived stem cells in 3D conditions - comparison of spheroids and polystyrene scaffolds, *Eur. Cell. Mater.* 37 (2019) 382–401, <https://doi.org/10.22203/eCM.v037a23>.
- [31] Z. Jamalpoor, M. Soleimani, N. Taromi, A. Asgari, Comparative evaluation of morphology and osteogenic behavior of human Wharton's jelly mesenchymal stem cells on 2D culture plate and 3D biomimetic scaffold, *J. Cell. Physiol.* 234 (2019) 23123–23134, <https://doi.org/10.1002/jcp.28876>.
- [32] S.K. Seidlits, J. Liang, R.D. Bierman, A. Sohrabi, J. Karam, S.M. Holley, C. Cepeda, C.M. Walthers, Peptide-modified, hyaluronic acid-based hydrogels as a 3D culture platform for neural stem/progenitor cell engineering, *J. Biomed. Mater. Res. A* 107 (2019) 704–718, <https://doi.org/10.1002/jbm.a.36603>.
- [33] D.L. Matera, K.M. DiLillo, M.R. Smith, C.D. Davidson, R. Parikh, M. Said, C. A. Wilke, I.M. Lombaert, K.B. Arnold, B.B. Moore, B.M. Baker, Microengineered 3D pulmonary interstitial mimetics highlight a critical role for matrix degradation in myofibroblast differentiation, *Sci. Adv.* 6 (2020), <https://doi.org/10.1126/sciadv.abb5069>.
- [34] P.M. Crapo, C.J. Medberry, J.E. Reing, S. Tottey, Y. van der Merwe, K.E. Jones, S. F. Badylak, Biologic scaffolds composed of central nervous system extracellular matrix, *Biomaterials* 33 (2012) 3539–3547, <https://doi.org/10.1016/j.biomaterials.2012.01.044>.
- [35] K. Pogoda, R. Bucki, F.J. Byfield, K. Cruz, T. Lee, C. Marcinkiewicz, P.A. Janney, Soft substrates containing hyaluronan mimic the effects of increased stiffness on morphology, motility, and proliferation of glioma cells, *Biomacromolecules* 18 (2017) 3040–3051, <https://doi.org/10.1021/acs.biomac.7b00324>.
- [36] H.W. Park, Y.C. Kim, B. Yu, T. Moroishi, J.-S. Mo, S.W. Plouffe, Z. Meng, K.C. Lin, F.-X. Yu, C.M. Alexander, C.-Y. Wang, K.-L. Guan, Alternative wnt signaling activates YAP/TAZ, *Cell* 162 (2015) 780–794, <https://doi.org/10.1016/j.cell.2015.07.013>.
- [37] G.M. Cunniffe, P.J. Diaz-Payno, E.J. Sheehy, S.E. Critchley, H.V. Almeida, P. Pitacco, S.F. Carroll, O.R. Mahon, A. Dunne, T.J. Levingstone, C.J. Moran, R. T. Brady, F.J. O'Brien, P.A.J. Brama, D.J. Kelly, Tissue-specific extracellular matrix scaffolds for the regeneration of spatially complex musculoskeletal tissues, *Biomaterials* 188 (2019) 63–73, <https://doi.org/10.1016/j.biomaterials.2018.09.044>.
- [38] G. Chu, Z. Yuan, C. Zhu, P. Zhou, H. Wang, W. Zhang, Y. Cai, X. Zhu, H. Yang, B. Li, Substrate stiffness- and topography-dependent differentiation of annulus fibrosus-derived stem cells is regulated by Yes-associated protein, *Acta Biomater.* 92 (2019) 254–264, <https://doi.org/10.1016/j.actbio.2019.05.013>.

- [39] J. Ma, Y. He, X. Liu, W. Chen, A. Wang, C.-Y. Lin, X. Mo, X. Ye, A novel electrospun-aligned nanoyarn/three-dimensional porous nanofibrous hybrid scaffold for annulus fibrosus tissue engineering, *Int. J. Nanomed.* 13 (2018) 1553–1567, <https://doi.org/10.2147/IJN.S143990>.
- [40] K. Li, D. Kapper, B. Youngs, V. Kocsis, S. Mondal, P. Kraus, T. Lufkin, Potential biomarkers of the mature intervertebral disc identified at the single cell level, *J. Anat.* 234 (2019) 16–32, <https://doi.org/10.1111/joa.12904>.
- [41] J.I. Sive, P. Baird, M. Jeziorski, A. Watkins, J.A. Hoyland, A.J. Freemont, Expression of chondrocyte markers by cells of normal and degenerate intervertebral discs, *Mol. Pathol.* 55 (2002) 91–97, <https://doi.org/10.1136/mp.55.2.91>.
- [42] C.R. Lee, D. Sakai, T. Nakai, K. Toyama, J. Mochida, M. Alini, S. Grad, A phenotypic comparison of intervertebral disc and articular cartilage cells in the rat, *Eur. Spine J. Off. Publ. Eur. Spine Soc. Eur. Spinal Deform. Soc. Eur. Sect. Cerv. Spine Res. Soc.* 16 (2007) 2174–2185, <https://doi.org/10.1007/s00586-007-0475-y>.
- [43] J. Rutges, L.B. Creemers, W. Dhert, S. Milz, D. Sakai, J. Mochida, M. Alini, S. Grad, Variations in gene and protein expression in human nucleus pulposus in comparison with annulus fibrosus and cartilage cells: potential associations with aging and degeneration, *Osteoarthritis Cartilage* 18 (2010) 416–423, <https://doi.org/10.1016/j.joca.2009.09.009>.
- [44] N. Fujita, T. Miyamoto, J. Imai, N. Hosogane, T. Suzuki, M. Yagi, K. Morita, K. Ninomiya, K. Miyamoto, H. Takaishi, M. Matsumoto, H. Morioka, H. Yabe, K. Chiba, S. Watanabe, Y. Toyama, T. Suda, CD24 is expressed specifically in the nucleus pulposus of intervertebral discs, *Biochem. Biophys. Res. Commun.* 338 (2005) 1890–1896, <https://doi.org/10.1016/j.bbrc.2005.10.166>.
- [45] J. Clouet, G. Grimandi, M. Pot-Vaucel, M. Masson, H.B. Fella, L. Guigand, Y. Cherel, E. Bord, F. Rannou, P. Weiss, J. Guicheux, C. Vinatier, Identification of phenotypic discriminating markers for intervertebral disc cells and articular chondrocytes, *Rheumatology* 48 (2009) 1447–1450, <https://doi.org/10.1093/rheumatology/kep262>.
- [46] B.M. Minogue, S.M. Richardson, L.A. Zeef, A.J. Freemont, J.A. Hoyland, Transcriptional profiling of bovine intervertebral disc cells: implications for identification of normal and degenerate human intervertebral disc cell phenotypes, *Arthritis Res. Ther.* 12 (2010) R22, <https://doi.org/10.1186/ar2929>.
- [47] B.P. Antunes, M.L. Vainieri, M. Alini, E. Monsonego-Ornan, S. Grad, A. Yayon, Enhanced chondrogenic phenotype of primary bovine articular chondrocytes in Fibrin-Hyaluronan hydrogel by multi-axial mechanical loading and FGF18, *Acta Biomater.* 105 (2020) 170–179, <https://doi.org/10.1016/j.actbio.2020.01.032>.
- [48] Y. Tao, X. Zhou, D. Liu, H. Li, C. Liang, F. Li, Q. Chen, Proportion of collagen type II in the extracellular matrix promotes the differentiation of human adipose-derived mesenchymal stem cells into nucleus pulposus cells, *Biofactors* 42 (2016) 212–223, <https://doi.org/10.1002/biof.1266>.
- [49] P.J. Roughley, L.I. Melching, T.F. Heathfield, R.H. Pearce, J.S. Mort, The structure and degradation of aggrecan in human intervertebral disc, *Eur. Spine J. Off. Publ. Eur. Spine Soc. Eur. Spinal Deform. Soc. Eur. Sect. Cerv. Spine Res. Soc.* 15 (Suppl 3) (2006) S326–S332, <https://doi.org/10.1007/s00586-006-0127-7>.
- [50] X. Lin, X. Fang, Q. Wang, Z. Hu, K. Chen, Z. Shan, S. Chen, J. Wang, J. Mo, J. Ma, W. Xu, A. Qin, S. Fan, Decellularized allogeneic intervertebral disc: natural biomaterials for regenerating disc degeneration, *Oncotarget* 7 (2016) 12121–12136, <https://doi.org/10.18632/oncotarget.7735>.
- [51] D.M. Varma, M.S. DiNicolas, S.B. Nicoll, Injectable, redox-polymerized carboxymethylcellulose hydrogels promote nucleus pulposus-like extracellular matrix elaboration by human MSCs in a cell density-dependent manner, *J. Biomater. Appl.* 33 (2018) 576–589, <https://doi.org/10.1177/0885328218805216>.
- [52] P. Colombier, J. Clouet, C. Boyer, M. Ruel, G. Bonin, J. Lesoeur, A. Moreau, B.-H. Fella, P. Weiss, L. Lescaudron, A. Camus, J. Guicheux, TGF-beta1 and GDF5 act synergistically to drive the differentiation of human adipose stromal cells toward nucleus pulposus-like cells, *Stem Cell.* 34 (2016) 653–667, <https://doi.org/10.1002/stem.2249>.
- [53] B.K. Bhunia, D.L. Kaplan, B.B. Mandal, Silk-based multilayered angle-ply annulus fibrosus construct to recapitulate form and function of the intervertebral disc, *Proc. Natl. Acad. Sci. U. S. A.* 115 (2018) 477–482, <https://doi.org/10.1073/pnas.1715912115>.
- [54] C. Zhu, J. Li, C. Liu, P. Zhou, H. Yang, B. Li, Modulation of the gene expression of annulus fibrosus-derived stem cells using poly(ether carbonate urethane)urea scaffolds of tunable elasticity, *Acta Biomater.* 29 (2016) 228–238, <https://doi.org/10.1016/j.actbio.2015.09.039>.
- [55] C.K.K. Choi, Y.J. Xu, B. Wang, M. Zhu, L. Zhang, L. Bian, Substrate coupling strength of integrin-binding ligands modulates adhesion, spreading, and differentiation of human mesenchymal stem cells, *Nano Lett.* 15 (2015) 6592–6600, <https://doi.org/10.1021/acs.nanolett.5b02323>.
- [56] D. Garcíadiego-Cázares, C. Rosales, M. Katoh, J. Chimal-Monroy, Coordination of chondrocyte differentiation and joint formation by alpha5beta1 integrin in the developing appendicular skeleton, *Development* 131 (2004) 4735–4742, <https://doi.org/10.1242/dev.01345>.
- [57] R.F. Loeser, S. Sadiev, L. Tan, M.B. Goldring, Integrin expression by primary and immortalized human chondrocytes: evidence of a differential role for alpha1beta1 and alpha2beta1 integrins in mediating chondrocyte adhesion to types II and VI collagen, *Osteoarthritis Cartilage* 8 (2000) 96–105, <https://doi.org/10.1053/joca.1999.0277>.
- [58] R.O. Hynes, Integrins: bidirectional, allosteric signaling machines, *Cell* 110 (2002) 673–687, [https://doi.org/10.1016/s0092-8674\(02\)00971-6](https://doi.org/10.1016/s0092-8674(02)00971-6).
- [59] V. Reyhani, P. Seddigh, B. Guss, R. Gustafsson, L. Rask, K. Rubin, Fibrin binds to collagen and provides a bridge for alpha3beta1 integrin-dependent contraction of collagen gels, *Biochem. J.* 462 (2014) 113–123, <https://doi.org/10.1042/BJ20140201>.
- [60] T. Hayashida, J.C.R. Jones, C.K. Lee, H.W. Schnaper, Loss of beta1-integrin enhances TGF-beta1-induced collagen expression in epithelial cells via increased alphavbeta3-integrin and Rac 1 activity, *J. Biol. Chem.* 285 (2010) 30741–30751, <https://doi.org/10.1074/jbc.M110.105700>.
- [61] S. Piccolo, S. Dupont, M. Cordenonsi, The biology of YAP/TAZ: hippo signaling and beyond, *Physiol. Rev.* 94 (2014) 1287–1312, <https://doi.org/10.1152/physrev.00005.2014>.
- [62] C.G. Hansen, T. Moroishi, K.-L. Guan, Yap, TAZ, A nexus for Hippo signaling and beyond, *Trends Cell Biol.* 25 (2015) 499–513, <https://doi.org/10.1016/j.tcb.2015.05.002>.
- [63] M.N. Barcellona, J.E. Speer, B.V. Fearing, L. Jing, A. Pathak, M.C. Gupta, J. M. Buchowski, M. Kelly, L.A. Setton, Control of Adhesive Ligand Density for Modulation of Nucleus Pulposus Cell Phenotype, Elsevier Ltd, 2020, <https://doi.org/10.1016/j.biomaterials.2020.120057>.
- [64] J.-Y. Shiu, L. Aires, Z. Lin, V. Vogel, Nanopillar force measurements reveal actin-mediated YAP mechanotransduction, *Nat. Cell Biol.* 20 (2018) 262–271, <https://doi.org/10.1038/s41556-017-0030-y>.
- [65] F.-X. Yu, B. Zhao, K.-L. Guan, Hippo pathway in organ size control, tissue homeostasis, and cancer, *Cell* 163 (2015) 811–828, <https://doi.org/10.1016/j.cell.2015.10.044>.
- [66] G. Halder, R.L. Johnson, Hippo signaling: growth control and beyond, *Development* 138 (2011) 9–22, <https://doi.org/10.1242/dev.045500>.
- [67] V. Fu, S.W. Plouffe, K.-L. Guan, The Hippo pathway in organ development, homeostasis, and regeneration, *Curr. Opin. Cell Biol.* 49 (2017) 99–107, <https://doi.org/10.1016/j.cob.2017.12.012>.
- [68] B. Yang, H. Sun, P. Chen, N. Fan, H. Zhong, X. Liu, Y. Wu, J. Wang, YAP1 influences differentiation of osteoblastic MC3T3-E1 cells through the regulation of ID1, *J. Cell. Physiol.* 234 (2019) 14007–14018, <https://doi.org/10.1002/jcp.28088>.
- [69] M. Bao, J. Xie, N. Katoe, X. Hu, B. Wang, A. Piruska, W.T.S. Huck, Cellular volume and matrix stiffness direct stem cell behavior in a 3D microniche, *ACS Appl. Mater. Interfaces* 11 (2019) 1754–1759, <https://doi.org/10.1021/acsami.8b19396>.
- [70] S. Lee, S. Kumar, Actomyosin stress fiber mechanosensing in 2D and 3D, *Fl000Research* 5 (2016), <https://doi.org/10.12688/fl000research.8800.1>.
- [71] Y.A. Miroshnikova, H.Q. Le, D. Schneider, T. Thalheim, M. Rubsam, N. Bremicker, J. Polleux, N. Kamprad, M. Tarantola, I. Wang, M. Balland, C.M. Niessen, J. Galle, S.A. Wickstrom, Adhesion forces and cortical tension couple cell proliferation and differentiation to drive epidermal stratification, *Nat. Cell Biol.* 20 (2018) 69–80, <https://doi.org/10.1038/s41556-017-0005-z>.
- [72] J.Y. Lee, J.K. Chang, A.A. Dominguez, H.-P. Lee, S. Nam, J. Chang, S. Varma, L. S. Qi, R.B. West, O. Chaudhuri, YAP-independent mechanotransduction drives breast cancer progression, *Nat. Commun.* 10 (2019) 1848, <https://doi.org/10.1038/s41467-019-09755-0>.
- [73] Q. Feng, H. Gao, H. Wen, H. Huang, Q. Li, M. Liang, Y. Liu, H. Dong, X. Cao, Engineering the cellular mechanical microenvironment to regulate stem cell chondrogenesis: insights from a microgel model, *Acta Biomater.* 113 (2020) 393–406, <https://doi.org/10.1016/j.actbio.2020.06.046>.
- [74] W. Zhang, Y. Kong, YAP is essential for TGF-beta-induced retinal fibrosis in diabetic rats via promoting the fibrogenic activity of Müller cells, *J. Cell Mol. Med.* 24 (2020) 12390–12400, <https://doi.org/10.1111/jcmm.15739>.
- [75] J. Jin, T. Wang, W. Park, W. Li, W. Kim, S.K. Park, K.P. Kang, Inhibition of yes-associated protein by verteporfin ameliorates unilateral ureteral obstruction-induced renal tubulointerstitial inflammation and fibrosis, *Int. J. Mol. Sci.* 21 (2020), <https://doi.org/10.3390/ijms21218184>.
- [76] R. Strippoli, P. Sandoval, R. Moreno-Vicente, L. Rossi, C. Battistelli, M. Terri, L. Pascual-Antón, M. Loureiro, F. Matteini, E. Calvo, J.A. Jiménez-Heffernan, M. J. Gómez, V. Jiménez-Jiménez, F. Sánchez-Cabo, J. Vázquez, M. Tripodi, M. López-Cabrera, M.A. Del Pozo, Caveolin 1 and YAP drive mechanically induced mesothelial to mesenchymal transition and fibrosis, *Cell Death Dis.* 11 (2020) 647, <https://doi.org/10.1038/s41419-020-02822-1>.
- [77] C. Shu, S.M. Smith, C.B. Little, J. Melrose, Use of FGF-2 and FGF-18 to direct bone marrow stromal stem cells to chondrogenic and osteogenic lineages, *Futur. Sci. OA.* 2 (2016) FSO142, <https://doi.org/10.4155/fsoa-2016-0034>.
- [78] L.J. Dawes, E.J. Shelley, J.W. McAvoy, F.J. Lovicu, A role for Hippo/YAP-signaling in FGF-induced lens epithelial cell proliferation and fibre differentiation, *Exp. Eye Res.* 169 (2018) 122–133, <https://doi.org/10.1016/j.exer.2018.01.014>.
- [79] P. Grunert, B.H. Borde, S.B. Towne, Y. Moriguchi, K.D. Hudson, L.J. Bonassar, R. Hartl, Riboflavin crosslinked high-density collagen gel for the repair of annular defects in intervertebral discs: an in vivo study, *Acta Biomater.* 26 (2015) 215–224, <https://doi.org/10.1016/j.actbio.2015.06.006>.
- [80] X. Zhou, J. Wang, W. Fang, Y. Tao, T. Zhao, K. Xia, C. Liang, J. Hua, F. Li, Q. Chen, Genipin cross-linked type II collagen/chondroitin sulfate composite hydrogel-like cell delivery system induces differentiation of adipose-derived stem cells and regenerates degenerated nucleus pulposus, *Acta Biomater.* 71 (2018) 496–509, <https://doi.org/10.1016/j.actbio.2018.03.019>.
- [81] P. Colombier, J. Clouet, O. Hamel, L. Lescaudron, J. Guicheux, The lumbar intervertebral disc: from embryonic development to degeneration, *Joint Bone Spine* 81 (2014) 125–129, <https://doi.org/10.1016/j.jbspin.2013.07.012>.
- [82] E.S. Silagi, I.M. Shapiro, M.V. Risbud, Glycosaminoglycan synthesis in the nucleus pulposus: dysregulation and the pathogenesis of disc degeneration, *Matrix Biol.* 71–72 (2018) 368–379, <https://doi.org/10.1016/j.matbio.2018.02.025>.
- [83] H. Yang, J. Wu, J. Liu, M. Ebraheim, S. Castillo, X. Liu, T. Tang, N.A. Ebraheim, Transplanted mesenchymal stem cells with pure fibrinous gelatin-forming growth factor-beta1 decrease rabbit intervertebral disc degeneration, *Spine J.* 10 (2010) 802–810, <https://doi.org/10.1016/j.spinee.2010.06.019>.

- [84] H. Hong, H. Kim, S.J. Han, J. Jang, H.K. Kim, D.-W. Cho, D.S. Kim, Compressed collagen intermixed with cornea-derived decellularized extracellular matrix providing mechanical and biochemical niches for corneal stroma analogue, *Mater. Sci. Eng. C. Mater. Biol. Appl.* 103 (2019) 109837, <https://doi.org/10.1016/j.msec.2019.109837>.
- [85] M. Su, Q. Zhang, Y. Zhu, S. Wang, J. Lv, J. Sun, P. Qiu, S. Fan, K. Jin, L. Chen, X. Lin, Preparation of decellularized triphasic hierarchical bone-fibrocartilage-tendon composite extracellular matrix for enthesis regeneration, *Adv. Healthc. Mater.* 8 (2019), e1900831, <https://doi.org/10.1002/adhm.201900831>.
- [86] D.O. Visscher, H. Lee, P.P.M. van Zuijlen, M.N. Helder, A. Atala, J.J. Yoo, S.J. Lee, A photo-crosslinkable cartilage-derived extracellular matrix (ECM) bioink for auricular cartilage tissue engineering, *Acta Biomater.* 121 (2020) 193–203, <https://doi.org/10.1016/j.actbio.2020.11.029>.
- [87] T. Lin, S. Liu, S. Chen, S. Qiu, Z. Rao, J. Liu, S. Zhu, L. Yan, H. Mao, Q. Zhu, D. Quan, X. Liu, Hydrogel derived from porcine decellularized nerve tissue as a promising biomaterial for repairing peripheral nerve defects, *Acta Biomater.* 73 (2018) 326–338, <https://doi.org/10.1016/j.actbio.2018.04.001>.
- [88] R.E. Neuman, M.A. Logan, The determination of hydroxyproline, *J. Biol. Chem.* 184 (1950) 299–306.
- [89] L. Kang, Q. Xiang, S. Zhan, Y. Song, K. Wang, K. Zhao, S. Li, Z. Shao, C. Yang, Y. Zhang, Restoration of autophagic flux rescues oxidative damage and mitochondrial dysfunction to protect against intervertebral disc degeneration, *Oxid. Med. Cell. Longev.* 2019 (2019) 7810320, <https://doi.org/10.1155/2019/7810320>.
- [90] S. Chen, X. Lv, B. Hu, Z. Shao, B. Wang, K. Ma, H. Lin, M. Cui, RIPK1/RIPK3/MLKL-mediated necroptosis contributes to compression-induced rat nucleus pulposus cells death, *Apoptosis* 22 (2017) 626–638, <https://doi.org/10.1007/s10495-017-1358-2>.